Carbon-13 Nuclear Magnetic Resonance Investigations of Phase Transitions and Phase Equilibria in Pure and Mixed Phospholipid Bilayers†

R. J. Wittebort,‡ A. Blume,§ T.-H. Huang, S. K. Das Gupta, and R. G. Griffin*

ABSTRACT: The temperature dependence of the ^{13}C NMR spectra of dipalmitoylphosphatidylethanolamine (DPPE) and three lecithins—dimyristoyl-, dipalmitoyl-, and distearoylphosphatidylcholine—which have been ^{13}C-labeled at the *sn*-2 carbonyl has been studied. In the L_β or $L_{\beta'}$ phase, an axially symmetric powder pattern of about 100-ppm breadth is observed, and this transforms to an isotropic line at the main L_β ($L_{\beta'}$) → L_α phase transition. In the case of DPPE, this transformation occurs precipitously and, with data from ^2H spectra of ^2H chain labeled DPPE, is shown to be due to a change in conformation at the *sn*-2 carbonyl. In contrast, the $^{13}C{=}O$ *sn*-2 spectra of lecithins exhibit a gradual transformation, beginning at temperatures below the endothermic pretransition temperature. Thus, in the intermediate $P_{\beta'}$ phase, a temperature-dependent superposition of the $L_{\beta'}$- and L_α-like ^{13}C spectra is observed, suggesting that the $P_{\beta'}$ phase is structurally heterogeneous and exhibits properties of both the $L_{\beta'}$ and L_α phases. Simulation of the *sn*-2 $^{13}C{=}O$ powder patterns, assuming diffusion about the lipid long axis and exchange between the two conformations, provides excellent fits of the spectra. The rate constants for the exchange can be related to the lateral diffusion constants measured by other techniques, and there is good agreement between the two. Addition of cholesterol (CHOL) to the four pure lipids also results in a superposition of the L_β ($L_{\beta'}$) and L_α patterns, and simulation of the spectra provides a means to extract the fraction of L_α-like lipid as a function of temperature or CHOL concentration. Similar results are observed for binary mixtures of dipalmitoylphosphatidylcholine and DPPE, indicating that *sn*-2 carbonyl spectra should also be a useful probe for examining phase equilibria in multicomponent lipid mixtures. Collectively, the results suggest that the conformational change at the *sn*-2 C=O is a general property of phospholipid phase transitions.

A ubiquitous property of pure lipid bilayers is the existence of a thermotropic phase transition at a temperature (T_c) from an ordered (gel) phase to a disordered (liquid-crystalline) phase. As might be expected, the detailed nature of this transition depends on the structure of the lipid molecule—e.g., the acyl chain length and the nature of the polar head group—and it can also be strongly affected by the incorporation of additional components into the bilayer to form a multiple component lipid system (Lee, 1977). Moreover, there have been several studies which suggest that the function of biological membranes is at least partially controlled by the phase behavior of the lipids in the bilayer (Overath et al., 1975; Linden et al., 1973; Verkleij et al., 1972; Melchior & Steim, 1979; Racker et al., 1975; Overath & Thilo, 1978). For these reasons, phase transitions in pure lipid bilayers and phase transitions and equilibria in mixed-lipid systems have received a great deal of attention over the last decade.

Probably the most extensive studies of these phenomena have been performed with differential scanning calorimetry (DSC)[1] (Chapman et al., 1967) where a sharp endotherm of about 8 kcal/mol is generally observed for phospholipid bilayers of lipids with palmitoyl chains. In the past, this endotherm has primarily been associated with an order–disorder transition of the acyl chains. That is, in the gel state, the fatty acyl chains are thought to be in an all-trans conformation whereas in the liquid-crystalline phase there is a significant population of gauche isomers present. In agreement with this hypothesis, X-ray (Tardieu et al., 1973; Luzzatti, 1968; Janiak et al., 1976) and neutron diffraction (Büldt et al., 1979) experiments indicate that the bilayer spacing decreases on traversing the phase transition by ~10–15 Å, and this observation is most easily explained by assuming the existence of gauche isomers in the acyl chains of liquid-crystalline phase lipids. Freeze–fracture electron microscopy has also been useful in understanding the phase behavior of lipid bilayers. For example, some of the most convincing evidence for the existence of the monoclinic phase exhibited by pure lecithin bilayers in the temperature range between the pretransition and main transition comes from observation of ripples of ~120–140-Å period in the electron micrographs (Luna & McConnell, 1977). An additional approach to the examination of lipid phase behavior has been to covalently attach a paramagnetic spin or fluorescent probe to a lipid molecule or to dissolve such a probe in the bilayer and to examine the ESR or fluorescence spectrum as a function of temperature or composition (Shimshick & McConnell, 1973; Shinitzky et al., 1971; Shinitzky & Barenholz, 1978). Since the changes in the ESR or fluorescence spectrum are due to changes in the motional properties of the probe, this type of experiment can in principle lead to information on dynamic processes which occur in the bilayer under study.

The deficiency of most of these methods is that in general they provide only macroscopic and not microscopic information on the system under investigation. For example, if cholesterol is incorporated into a bilayer, it is generally observed that the

† From the Francis Bitter National Magnet Laboratory, Massachusetts Institute of Technology, Cambridge, Massachusetts 02139. *Received October 26, 1981.* This research was supported by the National Institutes of Health (GM-23289 and RR-00995) and by the National Science Foundation through its support of the Francis Bitter National Magnet Laboratory (C-670). A.B. was supported by a research scholarship from the Deutsche Forschungsgemeinschaft (BL 182/2-4) and R.J.W. by a U.S. Public Health Service Postdoctoral Fellowship (GM-07215).

‡ Present address: Department of Chemistry, University of Louisville, Louisville, KY 40292.

§ Present address: Institut für Physikalische Chemie II, D-7800 Freiburg, Federal Republic of Germany.

[1] Abbreviations: CHOL, cholesterol; DMPC, dimyristoylphosphatidylcholine; DPPC, dipalmitoylphosphatidylcholine; DSPC, distearoylphosphatidylcholine; DPPE, dipalmitoylphosphatidylethanolamine; NMR, nuclear magnetic resonance; DSC, differential scanning calorimetry; ESR, electron spin resonance.

0006-2960/82/0421-3487$01.25/0

DSC endotherm broadens (Ladbrooke et al., 1968), but it is not possible to associate this broadening with particular molecular events. It is this type of problem that makes spectroscopic investigations of lipid bilayers appealing, since with these techniques it is possible to detect changes in molecular structure and dynamics. It is undoubtedly partially for this reason that there have recently been a number of infrared and Raman investigations aimed at elucidating the structural properties of, for example, lecithin bilayers and the manner in which the properties change at the phase transition (Gaber & Peticolas, 1977; Gaber et al., 1978; Bansil et al., 1980; Cameron et al., 1981a,b; Sunder et al., 1981; Vogel & Jähnig, 1981).

Another obvious spectroscopic technique which could be employed in this type of investigation is nuclear magnetic resonance, and its appeal is evident by the numerous structural and dynamical investigations of lipid bilayers utilizing ^1H, ^2H, ^{13}C, and ^{31}P NMR spectra (Seelig, 1977; Seelig & Seelig, 1980; Jacobs & Oldfield, 1981; Griffin, 1981). To date, however, these investigations have been largely confined to the liquid-crystalline phase because of technical difficulties associated with the observation of gel-state lipid NMR spectra. For example, ^2H NMR spectra of the liquid-crystalline phase are relatively narrow, and thus easily observed, and as a consequence, they have been studied in a number of cases (Seelig, 1977). However, in the gel phase, the spectra are considerably wider, and only with recent improvements in NMR methodology have they become amenable to examination (Davis, 1979; Griffin, 1981). Thus, to date there have been only two reports which described ^2H NMR spectra of both the gel and liquid-crystalline phases of lecithin and glycolipid bilayers (Davis, 1979; Huang et al., 1980) and thus the phase transitions which occur in these systems. Nevertheless, with these advances in methodology, it should now be possible to perform NMR studies aimed at elucidating the molecular events associated with lipid phase transitions and equilibria in some detail.

In addition to these two deuterium NMR studies, we recently reported a ^{13}C NMR investigation of the gel to liquid-crystalline phase transition in dipalmitoylphosphatidylcholine (Wittebort et al., 1981). In this investigation, we examined the ^{13}C spectra of DPPC which had been isotopically labeled at the *sn*-2 carbonyl, and we observed rather dramatic alterations in the spectra on passing through the transition. In the low-temperature $L_{\beta'}$ gel phase, the *sn*-2 carbonyl exhibited an axially symmetric powder pattern of about 110-ppm breadth which collapsed to an isotropic-like line in the liquid-crystalline L_α phase. In the intermediate $P_{\beta'}$ phase, a temperature-dependent superposition of these spectra was observed. These observations suggested that similar experiments might be of utility in studies of other pure and mixed lipid bilayers, and in this paper, we report an investigation of this possibility. Specifically, we have examined the ^{13}C carbonyl spectra of pure bilayers of DMPC, DSPC, and DPPE as a function of temperature. All three of the lipids exhibit the behavior reported previously for DPPC; e.g., the $L_{\beta'}$ powder pattern transforms to a narrow line in the L_α phase. Moreover, in the monoclinic phase of the lecithins, a superposition of these spectra is observed. In addition, we have investigated the ^{13}C spectra of DMPC labeled at the *sn*-1 carbonyl. Finally, we present preliminary data on the effect of CHOL on the spectra of the PC's and DPPE, and in addition spectra of a binary mixture of DPPC and DPPE.

Experimental Procedures

Lipid Synthesis. [1-^{13}C]Myristic, palmitic, and stearic acids were synthesized by reaction of a long-chain bromide with $^{13}C{\equiv}N$ and subsequent hydrolysis to the fatty acid or were purchased from Kor Isotopes (Cambridge, MA). The synthesis of ^2H-labeled fatty acids is discussed elsewhere (Das Gupta et al., 1982). Phosphatidylcholines labeled at the carbonyl carbon of the *sn*-2 chain, for example, 2-[1-^{13}C]-DPPC, were prepared by acylation of the corresponding lysophosphatidylcholine with the fatty acid anhydride by using *N*,*N*-dimethyl-4-aminopyridine as a catalyst (Gupta et al., 1977). ^{13}C- and ^2H-labeled dipalmitoylphosphatidylethanolamine was synthesized similarly, except that the head group was blocked with *tert*-butyloxycarbonyl before the lyso-PE was prepared (Chakrabarti & Khorana, 1975). 1-[1-^{13}C]DMPC was synthesized by first preparing 1,2-[1-^{13}C]DMPC, converting this to lyso-PC, and then reacylating, according to the procedure of Boss et al. (1975). The NMR spectra indicate that significant amounts of chain migration accompanied this procedure. Purity was routinely checked with TLC on silica gel plates.

Sample Preparation. Samples for the NMR experiments generally consisted of approximately 50 mg of lipid dispersed in an equal weight of H_2O [^2H-depleted H_2O (Aldrich Chemicals, Milwaukee, WI) in the case of the ^2H spectra] which were sealed in 7-mm glass tubes for the NMR experiments. TLC's were generally taken after completion of the experiments to check for decomposition. In the case of lecithins, differential scanning calorimetry experiments were performed at Boston University on a Perkin-Elmer DSC-2 to ensure that the lipids exhibited a pretransition.

NMR Spectroscopy. ^{13}C and ^2H NMR spectra were obtained on a home-built pulse spectrometer operating at 73.9 MHz for ^{13}C and at 45.1 MHz for ^2H, corresponding to a ^1H frequency of 294 MHz. In most cases, the ^{13}C spectra were recorded with a Hahn echo which circumvents problems with receiver overload and acoustic probe ringing and thus yields undistorted powder spectra. In many cases, the spectral effects observed are strongly temperature dependent. Consequently, we were particularly careful to keep the ^1H decoupling power at the minimum level necessary to obtain well-resolved lines and thus, insofar as possible, to avoid sample heating. Recycle delays in the ^{13}C experiments were typically 5 s which helped to further minimize this problem. The ^{13}C $\pi/2$ pulse was $\simeq 3$ μs. All shifts are referenced to external benzene. ^2H NMR spectra were obtained with a two-pulse quadrupole echo (Solomon, 1958; Davis et al., 1976) using a $\pi/2$ pulse of 1.7 μs. Phase cycling was used in both echo experiments, and in both cases quadrature phase detection was employed.

Results

Shown on the right of Figure 1 are ^2H NMR spectra of 2-[4,4-$^2H_2$]DPPE/50 wt % H_2O as a function of temperature from 1 to 68 °C, and on the left of this figure are computer simulations of these spectra. At low temperatures (1 °C), the spectrum is 120 kHz wide and exhibits a more or less flat top with some structure. As the temperature is raised, the spectrum first transforms to a round shape, and at yet higher temperatures (23–45 °C), the central portion narrows and shoulders appear which are similar to those observed in axially symmetric powder spectra. At 55 °C, these shoulders are well-defined and separated by about 110 kHz, and a dip is present in the center of the spectrum. At the higher temperatures, the center of the spectrum narrows to a width of about 56 kHz. Finally, at 64 °C, the lipid undergoes a phase transition from the L_β to the L_α phase, where an axially symmetric spectrum with $\Delta\nu_{Q\perp} \simeq 30$ kHz is observed. On

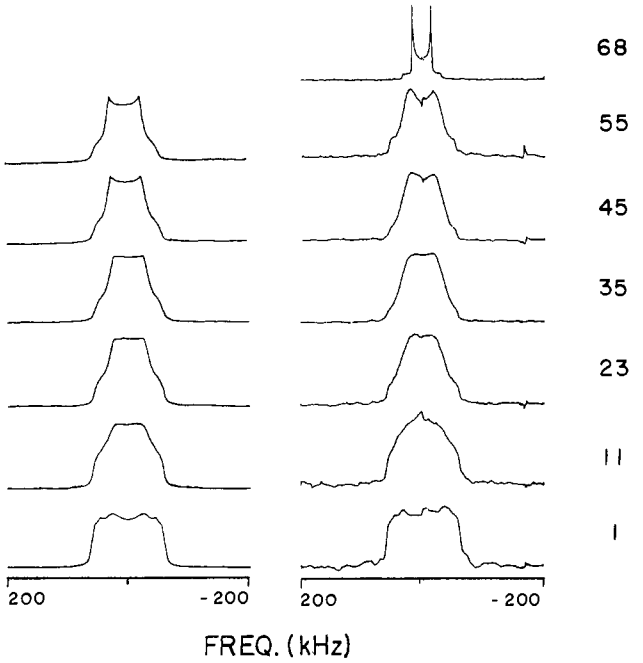

FIGURE 1: ^{2}H NMR spectra at 45.1 MHz of 2-[4,4-$^2H_2$]DPPE/50 wt % H_2O as a function of temperature (°C) (right) and computer simulations of these spectra (left). The simulations were performed with a program described in the text which assumes long axis diffusion and trans–gauche isomerization. The input parameters used in the simulations are as follows: R, the axial hopping rate; R_{tg}, the trans–gauche isomerization rate; P_t, the population of the trans state. At each temperature they are, respectively, the following: (1 °C) 2.1×10^5 s^{-1}, 2.7×10^4 s^{-1}, and 0.98; (11 °C) 3×10^5 s^{-1}, 3×10^4 s^{-1}, and 0.96; (23 °C) 4.5×10^5 s^{-1}, 4×10^4 s^{-1}, and 0.95; (35 °C) 5×10^5 s^{-1}, 5.4×10^4 s^{-1}, and 0.94; (45 °C) 6.25×10^5 s^{-1}, 7.3×10^4 s^{-1}, and 0.94; (55 °C) 7.5×10^5 s^{-1}, 8.5×10^4 s^{-1}, and 0.93.

the left of Figure 1 are computer simulations of these spectra which are based on a model which assumes 3-fold jumps of the lipid molecule about its long axis with superimposed trans–gauche isomerization. The rate of the long axis jumps, the trans–gauche isomerization rate, and the population of the trans state at each temperature are given in the figure caption. The simulations include corrections for power roll off (Bloom et al., 1980) and distortions due to the use of the quadrupole echo (Spiess & Sillescu, 1981). These spectra will be discussed in more detail below, but the important point to note is that the axial jumping rate ranges from 2.1×10^5 s^{-1} at 1 °C to 7.5×10^5 s^{-1} at 55 °C.

In Figure 2 are shown a series of proton-decoupled ^{13}C spectra of 2-[1-^{13}C]DPPE/50 wt % H_2O as a function of temperature from 1 to 69 °C. The broad band on the right side of these spectra (65–146 ppm) arises from the natural-abundance ^{13}C of the acyl chains, and immediately to its left are small signals due to the head-group and glycerol backbone carbons. The most prominent feature of these spectra is the powder pattern from the ^{13}C-enriched *sn*-2 C=O which extends from about −100 to 0 ppm. At −55 °C, this pattern is axially asymmetric with principal values $\sigma_{11} = -133$, $\sigma_{22} = -13$, and $\sigma_{33} = +11$ ppm, which are characteristic of a rigid lattice ester carbonyl tensor. At temperatures above 0 °C, the spectrum narrows to an axially symmetric pattern of about 95–100-ppm breadth; for example, at 45 °C, $\sigma_{\parallel} = -110$, $\sigma_{\perp} = -15$, and $|\Delta\sigma| = 95$ ppm. At 63 °C, which is 1 °C below T_c, a superposition of a broad powder pattern and an isotropic-like line is observed, and finally for $T > T_c$ (69 °C), the carbonyl pattern has collapsed to a narrow line of 2-ppm width, with a shift of $(1/3)\,\mathrm{Tr}(\bar{\sigma}) = -47$ ppm. The temperature dependence of these spectra, together with the ^{2}H spectra

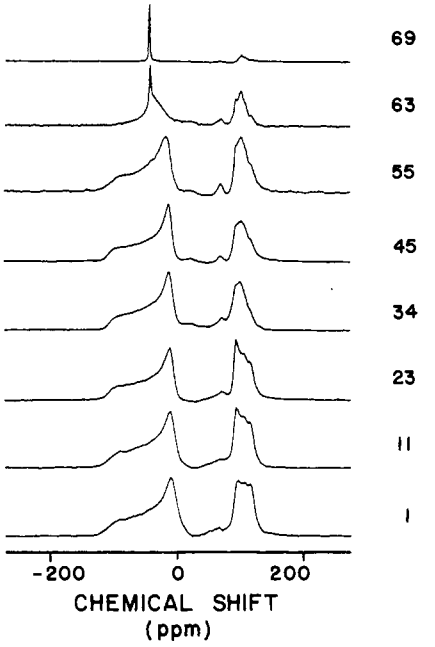

FIGURE 2: Proton-decoupled ^{13}C spectra of 2-[1-^{13}C]DPPE/50 wt % H_2O as a function of temperature (°C). Note the precipitous collapse of the *sn*-2 powder pattern to an isotropic line at the phase transition temperature (64 °C).

of Figure 1, suggests that the narrowing of the *sn*-2 carbonyl powder observed with increasing temperature of the L_β phase ($T < 64$ °C) is due to diffusion of the DPPE molecules about their long axis. From the ^{2}H spectra, we know the axial jump rate is approximately 5×10^5 s^{-1}, which is fast on the ^{13}C time scale, and thus the *sn*-2 carbonyl patterns are fast limit spectra. That is, their breadth is determined by the orientation of the tensor relative to the diffusion axis. The *sn*-2 carbonyl pattern collapses to an isotropic line upon passing through the phase transition. Since the axial diffusion rate is already greater than the breadth of the rigid lattice tensor, this must be due to a change in the orientation of the ^{13}C tensor with respect to the diffusion axis. In other words, formation of the L_α liquid-crystalline phase results in a conformational change at the *sn*-2 carbonyl which fortuitously tilts this tensor to the "magic angle" [$\theta = \cos^{-1}(1/3^{1/2})$] and results in an isotropic line.

In Figures 3–5, we show proton-decoupled ^{13}C spectra of 2-[1-^{13}C]DMPC, 2-[1-^{13}C]DPPC, and 2-[1-^{13}C]DSPC/50 wt % H_2O samples as a function of temperature. As can be discerned from these spectra, they bear some similarities to the ^{13}C spectra of 2-[1-^{13}C]DPPE discussed above. For example, in the $L_{\beta'}$ phase, an axially symmetric *sn*-2 carbonyl powder pattern is observed, in this case of ~110-ppm breadth, and this powder pattern collapses to an isotropic line in the L_α phase for all three PC's. Nevertheless, there are some notable differences. In the DPPE spectra, a superposition of the L_β and L_α spectra was seen only at temperatures within the main calorimetric phase transition. However, in the case of DMPC and DPPC, a superposition of these spectra is evident at temperatures 10–15 °C below T_c. For example, in the DMPC spectra, the superposition is discernible at 7 °C ($T_c = 23.5$ °C), and in DPPC, it appears at 27 °C ($T_c = 41.5$ °C). In the case of DSPC, the spectrum at 47 °C shows a hint of two components, but at 54 °C, they are both clearly visible. We believe these multicomponent spectra are due to the presence of the rippled P_β or $P_{\beta'}$ monoclinic phase which is displayed by pure lecithins.[2]

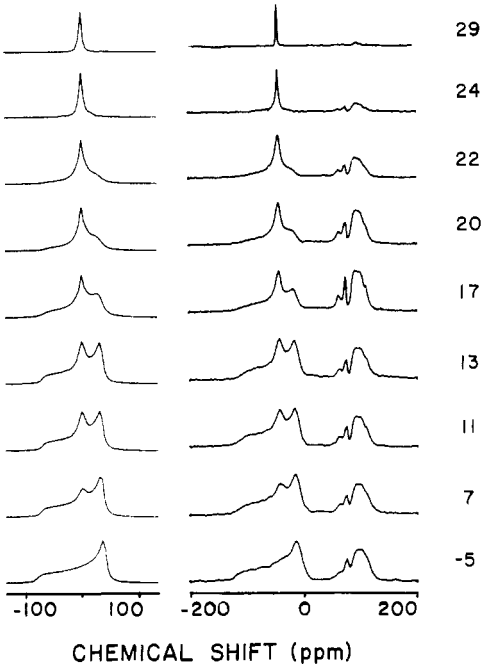

FIGURE 3: Experimental proton decoupled ^{13}C spectra of 2-[1-^{13}C]DMPC as a function of temperature (°C) (right) together with computer simulations of the *sn*-2 region of the spectrum (left). The simulations were performed with a computer program described in the text. Simulation parameters are included in Table III.

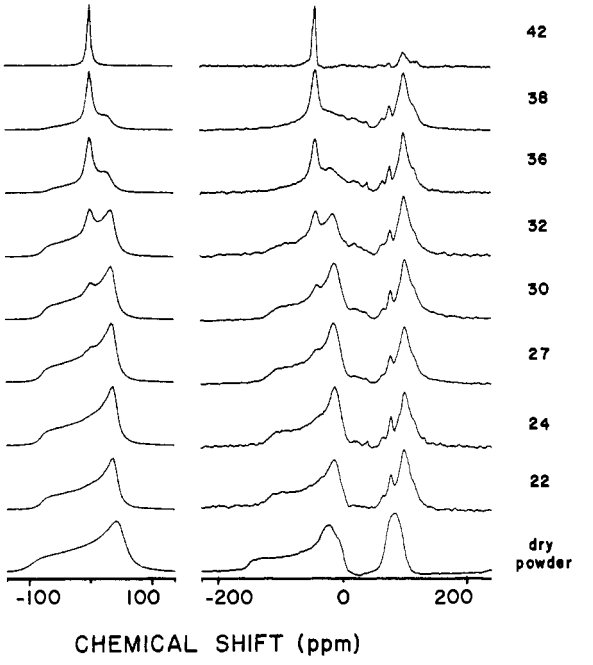

FIGURE 4: Experimental proton decoupled ^{13}C spectra of 2-[1-^{13}C]DPPC as a function of temperature (°C) (right) together with computer simulations of the *sn*-2 region of the spectrum (left). The dry powder spectrum (bottom trace) shows the slight asymmetry of the $^{13}C{=}O$ powder pattern observed for all the lecithins and DPPE. An identical spectrum is obtained from frozen aqueous dispersions. Simulation parameters are included in Table III.

Also shown in Figures 3–5 are computer simulations of the *sn*-2 carbonyl portion of the spectra. These simulations were performed with a computer program which assumed two types of axially symmetric $^{13}C{=}O$ tensors. The first is tilted at an angle of ~28° with respect to the diffusion axis, $\hat{D}$, while the second was at 54° with respect to this axis. Both tensors were allowed to execute rapid 3-fold jumps about $\hat{D}$, and in addition, there is exchange between the two tensor orientations. Although this model is quite simple, it does suffice to produce very good simulations of the spectra as can be seen by comparison of the simulations with the experimental results in Figures 3–5. Table III contains the data used for these simulations, which will be discussed further below.

We have also studied ^{13}C spectra of 1-[1-^{13}C]DMPC, and these are shown as a function of temperature in Figure 6. In the $L_{\beta'}$ phase, an axially symmetric pattern similar to that seen for the *sn*-2 carbonyl is observed, but in the L_α phase, the spectrum is quite different. Instead of the narrow isotropic line there is a powder pattern of reduced breadth, which as is shown narrows further with increasing temperature. However, in the $P_{\beta'}$ phase, there are clearly two powder patterns present, and we have marked the perpendicular edges of these patterns with a dashed line. Since the powder patterns are of similar width, the parallel edges of the spectra are not well resolved. There is also an *sn*-2 chain component visible in these spectra, particularly in the 29 °C spectrum, and this is due to the chain migration which occurred during the reacylation of the 1-^{13}C-labeled lyso compound.

We have also investigated the effects of other lipids on the *sn*-2 carbonyl spectra as is illustrated in Figures 7–11. On the right of Figure 7 are shown spectra of a 2-[1-^{13}C]DPPE in the presence of 20 mol % CHOL. At low temperature (1 °C), an axially symmetric powder pattern similar to that seen in the L_β phase of the pure lipid is observed, and at high temperatures ($T > 55$ °C), we again find the narrow isotropic spectrum. In the case of the pure 2-[1-^{13}C]DPPE, the axially symmetric L_β pattern was maintained up to the L_α phase transition temperature (cf. Figure 2), but we see that in the presence of CHOL this is not the case. Instead, in the tem-

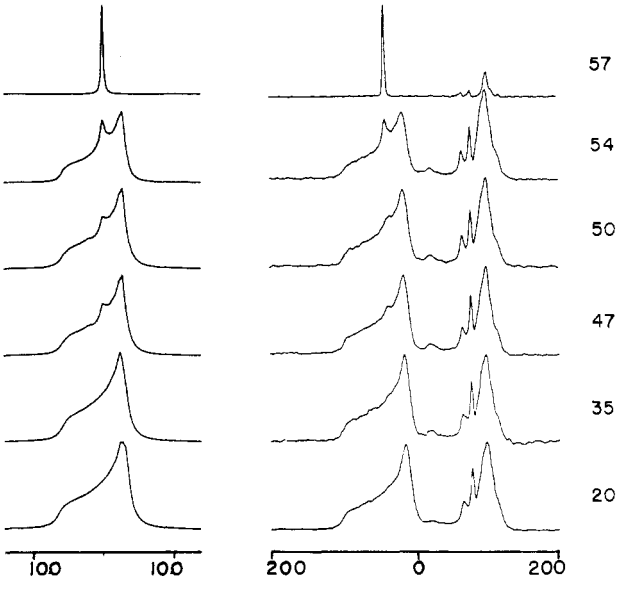

FIGURE 5: Experimental proton decoupled ^{13}C spectra of 2-[1-^{13}C]DSPC as a function of temperature (°C) (right) together with computer simulations (left). Simulation parameters are not given since only one spectrum (54 °C) shows a large L_α fraction. This is due to the narrow (3.4 °C) pretransition range in DSPC.

[2] The exact structure of the monoclinic ripple phase is a topic currently under investigation. While it is generally agreed that it is rippled, it is apparently not clear whether or not the chains are tilted. Janiak et al. (1976, 1979) refer to the phase as $P_{\beta'}$ (tilted) while, for example, Stamatoff et al. (1981) seem to believe P_β (untilted) is more appropriate. In this paper, we use the term $P_{\beta'}$ in reference to the rippled phase since its use is more common. However, we do not endorse it over P_β as being a correct description of the ripple phase.

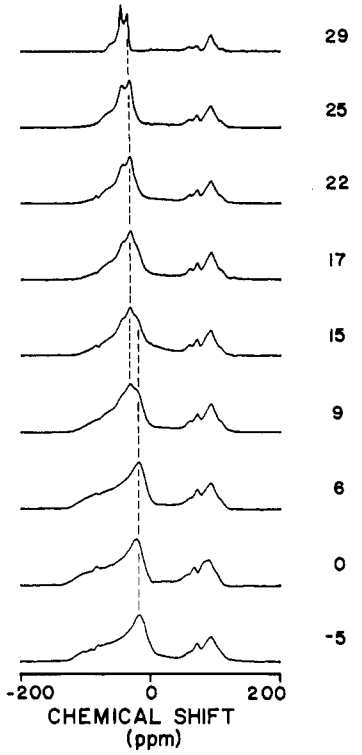

FIGURE 6: Proton-decoupled ^{13}C spectra of 1-[1-^{13}C]DMPC as a function of temperature (°C). Since the *sn*-1 ^{13}C=O patterns are similar in breadth in both the $L_{\beta'}$ and L_α phases, the superposition of spectra observed in the $P_{\beta'}$ region is not so well resolved as in the *sn*-2 case. Nevertheless, overlapped spectra are seen, and the position of the perpendicular edge is marked with a dashed line. There is an *sn*-2 component present due to chain migration.

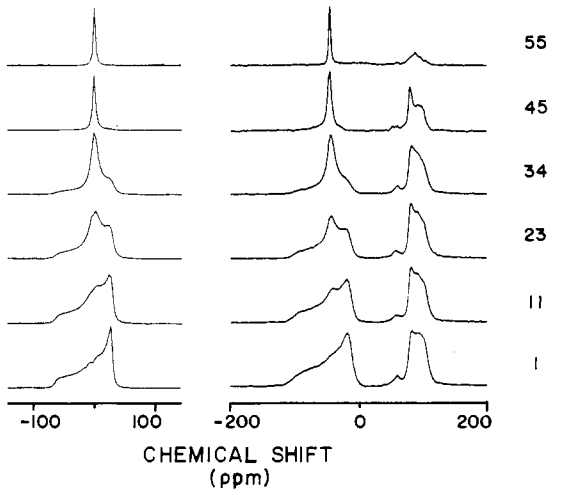

FIGURE 7: Experimental proton decoupled ^{13}C spectra of a 2-[1-^{13}C]DPPE/20 mol % CHOL mixture as a function of temperature (°C) (right) together with computer simulations of the spectra (left). Simulation parameters are included in Table IV.

perature range 11–45 °C, a clear superposition of the L_α and L_β spectra is evident, and the L_α spectrum grows in intensity with increasing temperature. On the left of Figure 7 are computer simulations of these spectra performed with the six-site chemical exchange program described below, and it is evident that the experimental results can be reproduced quite well with this model. In agreement with calorimetric studies, the addition of CHOL lowers the transition temperature of pure DPPE (Blume, 1980), and this is evident from the ^{13}C spectra since the L_α line appears at much lower temperature. Inside the calorimetrically observed transition region, the

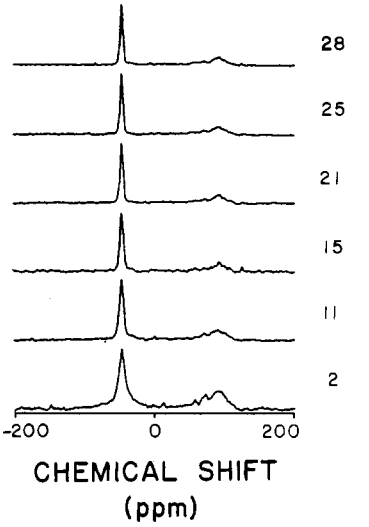

FIGURE 8: Experimental proton decoupled ^{13}C spectra of a 2-[1-^{13}C]DMPC/25 mol % CHOL mixture as a function of temperature (°C). In contrast to DPPE or the other lecithins, DMPC exhibits only the L_α line at all temperatures.

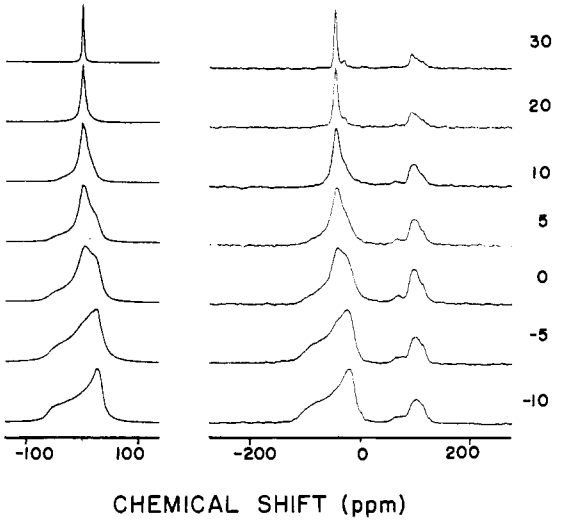

FIGURE 9: Proton-decoupled ^{13}C spectra of 2-[1-^{13}C]DPPC/30 mol % CHOL as a function of temperature (right) together with computer simulations of the *sn*-2 C=O region (left). Parameters used in the simulations are included in Table IV. A small *sn*-1 component is present (30 °C) because of chain migration.

spectra show two components. The spectra therefore indicate that inside the transition region the PE molecules can exhibit two different conformations, namely, $L_{\beta'}$- and L_α-like. Moreover, the rate of the exchange can be measured, and in the case, it is about (3–7) × 10^2 s^{-1} in the temperature range 11–45 °C.

The effect of CHOL on the ^{13}C spectra of *sn*-2 carbonyl labeled lecithins is illustrated in Figures 8–10. Shown in Figure 8 are spectra for 2-[1-^{13}C]DMPC at 25 mol % CHOL as a function of temperature. At all temperatures, only the isotropic L_α spectrum is observed, although the width of the line is broader than is seen in pure DMPC above T_c (cf. Figure 3). For this particular lipid, it is evident that 25 mol % CHOL suffices to induce a conformational change at the *sn*-2 C=O for a large fraction of lipid molecules down to temperatures of 0 °C. In Figures 9 and 10 are shown spectra of 2-[1-^{13}C]DPPC and 2-[1-^{13}C]DSPC at 30 mol % CHOL. In the case of DPPC, the L_α spectrum is observed at all temperatures above approximately 20 °C, and for DSPC the corresponding behavior is seen for temperatures greater than approximately

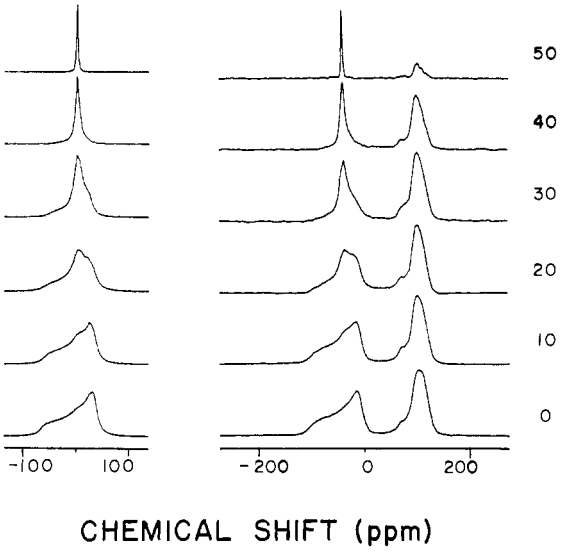

FIGURE 10: Proton-decoupled ^{13}C spectra of 2-[1-^{13}C]DSPC/30 mol % CHOL as a function of temperature (°C) (right) together with computer simulations of the *sn*-2 C=O region (left). The parameters employed in the simulation are included in Table IV.

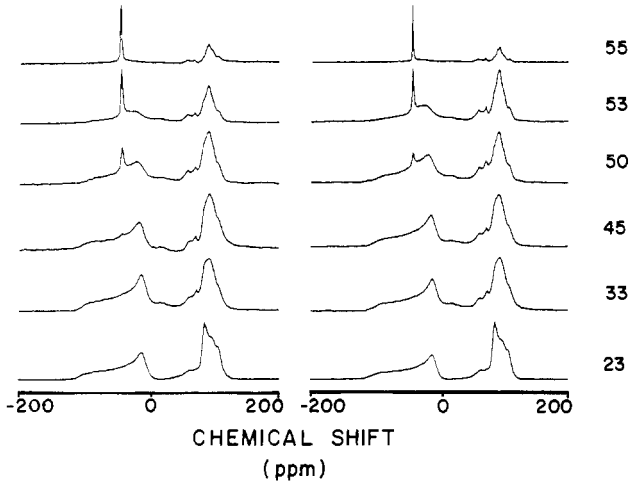

FIGURE 11: Proton-decoupled ^{13}C spectra of 1:1 mixtures of DPPC/DPPE (50 wt % H_2O) as a function of temperature (°C). (Left) 2-[1-^{13}C]DPPC/DPPE; (right) DPPC/2-[1-^{13}C]DPPE. In the temperature range 45–55 °C a clear superposition of L_β and L_α spectral patterns is observed.

40 °C. However, in contrast to DMPC, the spectra of both DPPC and DSPC exhibit the superposition of the L_α and $L_{\beta'}$ spectra at lower temperatures. For DPPC, the two-component spectrum is evident at temperatures between 0 and 20 °C, and for DSPC, the superposition is observed between approximately 20 and 40 °C at this CHOL concentration. As can be seen from Figures 9 and 10, the $L_{\beta'}$ pattern is recovered below 0 °C for DPPC and below 20 °C for DSPC. Also shown on the left of Figures 9 and 10 are computer simulations of the spectra, again assuming chemical exchange between L_α and $L_{\beta'}$ components, and there is excellent agreement between the two. The exchange rates obtained in both cases are approximately 10^2–10^3 s^{-1}, which is similar to that found for DPPE/CHOL mixtures.

We have also investigated the effect of DPPE on the ^{13}C spectra of DPPC and vice versa, and some preliminary results are illustrated in Figure 11. The spectra in this figure are for a 1:1 molar mixture of these two phospholipids, those on the left being for a 2-[1-^{13}C]DPPC/DPPE mixture while those on the right are for DPPC/2-[1-^{13}C]DPPE. The L_β axially symmetric pattern is evident in both sets of spectra at low temperatures, while above 55 °C the narrow L_α line is seen. This is in agreement with the idea that phases below and above these temperatures correspond to "solid" and "fluid" regions of the DPPC/DPPE phase diagram (Shimshick & McConnell, 1973; Blume & Ackermann, 1974). Moreover, when both L_α- and $L_{\beta'}$-like phases are simultaneously present, it is expected that a superposition of the L_α and L_β spectra would be observed. Inspection of Figure 11 shows that indeed this is the case for temperatures between 45 and 55 °C. For example, in the 2-[1-^{13}C]DPPC/DPPE spectra, a hint of the L_α line is seen at 45 °C, and it is clearly evident at 50 and 53 °C, where it is superimposed on the L_β pattern. In the DPPC/2-[1-^{13}C]DPPE spectra on the right, the L_α line is easily seen at 50 and 53 °C, but only the L_β pattern is observed at 45 °C. Since DPPC has a lower melting temperature than DPPE, this is the expected behavior. Note also that the L_α line in these spectra is much sharper than that observed in the PC or PE/CHOL mixtures which requires that exchange between pure and mixed domains is slower. In addition, the observation of these overlapping spectra suggests that they could be used to determine the phase diagram of these lipid mixtures, and we will see below that with some qualifications this is indeed the case.

Discussion

Under Results and in what follows, we use the term "L_α line" to describe the sharp component which appears in the *sn*-2 ^{13}C=O spectra of lecithins in the $P_{\beta'}$ phase (see Figures 3–5). In order to avoid confusion and misunderstandings, we would like at the outset to define our usage of this term. This usage is derived from the fact that the L_α phase invariably exhibits a sharp line, whereas the axially symmetric powder pattern is seen in the $L_{\beta'}$ phase. The temperature-dependent superposition of these spectra observed in the $P_{\beta'}$ phase implies that this intermediate phase possesses *some* features of both the L_α and $L_{\beta'}$ phases. That this is certainly the case is illustrated by *sn*-2 ^{13}C=O spectra discussed here. However, presently available evidence suggests that it would be naive to consider this phase as simply a mixture of L_α and $L_{\beta'}$ regions, and it is this point which we would like to emphasize. For example, ^2H NMR spectra of chain-labeled lecithins obtained in the pretransition region appear to be two-component spectra. However, they are broad and, except for temperatures near the main transition, lack the well-resolved features observed in a pure L_α phase (Blume et al., 1982). Thus, when we refer to the L_α line in the ^{13}C spectra reported here, we assume an operational definition of what constitutes L_α. This definition includes a correlation time which satisfies eq 2 below and the conformational change at the *sn*-2 C=O which is also discussed below. These comments are also applicable to lipid/CHOL and lipid/lipid mixtures where a similar superposition of spectra is also observed. However, this definition is not necessarily appropriate for other spectroscopic techniques, e.g., ^2H NMR.

Dipalmitoylphosphatidylethanolamine. In order to discuss the results presented above, we must first explain the origin of the collapse of the axially symmetric ^{13}C powder pattern observed in the L_β or $L_{\beta'}$ phases of PE or PC to the narrow line observed in the L_α phase of both lipids. As we have outlined previously (Wittebort et al., 1981), there are in the case of PC's several possible explanations of this phenomenon, and this "multiplicity" arises because of the occurrence of the $P_{\beta'}$ monoclinic phase between the $L_{\beta'}$ and L_α phases. However, if for the moment we restrict our attention to PE's which do not display a $P_{\beta'}$ phase, and the spectra of Figures 1 and 2,

we will see that there is an unambiguous interpretation of the results. In particular, the collapse of the powder pattern at the phase transition must involve a conformational change at the *sn*-2 carbonyl which fortuitously tilts the tensor to the magic angle.

There are two mechanisms by which a powder pattern such as is seen in all of the ^{13}C spectra shown above can be narrowed to an isotropic line. In the first model, we assume that the unique axis of the axially symmetric shielding tensor is oriented at the magic angle, 54.7°, with respect to diffusion axis in both the L_β and L_α phases. Given this orientation, the narrowing is then accomplished by invoking a change in the rate and/or amplitude of the thermally activated long axis diffusion in traversing the phase transition. Specifically, in the L_β phase, the correlation time for the motion, τ_c, is such that

$$\gamma H_0 \Delta\sigma \tau_c > 1 \quad (1)$$

and the $\Delta\sigma$ = 95 ppm powder pattern is observed. Correspondingly, if the correlation time is short, e.g.

$$\gamma H_0 \Delta\sigma \tau_c < 1 \quad (2)$$

the spectrum collapses to the narrow isotropic L_α phase spectrum. In the intermediate motional regime where

$$\gamma H_0 \Delta\sigma \tau_c \approx 1 \quad (3)$$

the line shapes depend on the correlation times and the details of the motional model.

The motion about the long axis can assume at least two forms, and these are continuous or small angle jump diffusion or alternatively large angle jump diffusion. The continuous or small angle jump motional mode has been discussed previously (Wittebort et al., 1981) and results in line shapes which exhibit well-resolved edges only in the limit of slow or rapid diffusion. In the intermediate rate regime, the line shapes are broadened and thus inconsistent with the L_β phase ^{13}C spectra of Figure 2. Thus, if this model were correct, then it would be necessary to have long axis diffusion rates of 10^2–10^3 s^{-1} in the L_β phase, and such rates would lead to axially symmetric ^{2}H powder patterns of about twice the width of those shown in Figure 1. For this reason, we exclude this model from further consideration.

If we assume that the motion involves large angle jump diffusion, then line shapes such as are shown in Figure 12 result. For these simulations, we have oriented the unique axis of an axially symmetric tensor of 12-kHz breadth at the magic angle, and we let it execute 3-fold hops about the molecular long axis. At slow hopping rates, the axially symmetric powder pattern is observed, and for fast hops, the spectrum collapses to the isotropic line. In the intermediate regime, there is a spike which grows in intensity with the hopping rate and results in spectra which bear some similarities to those shown above for pure PC's and for PE/CHOL, PC/CHOL, and PC/PE mixtures. The behavior illustrated in Figure 12—e.g., the simultaneous presence of sharp patterns for both the original and motionally averaged spectrum in the intermediate exchange region—is a characteristic of discrete motion spectra. Nevertheless, we can exclude this model as a plausible explanation of our PE spectra for the following reasons. First, the size of the sharp component is quantitatively different from that seen in the experimental spectra. Second, the sharp component at the isotropic resonance frequency appears for hopping rates of $\sim 10^3$–10^4 s^{-1}, and for rates $>10^4$ s^{-1}, it alone is observed. From the ^{2}H chain labeled spectra of Figure 1, we know that the axial jumping rate must be $>10^5$ s^{-1} for temperatures between 1 and 55 °C. Thus, if this model were correct, the ^{13}C spectra of Figure 2 would consist of only the narrow line observed in the L_α phase rather than the 95-ppm

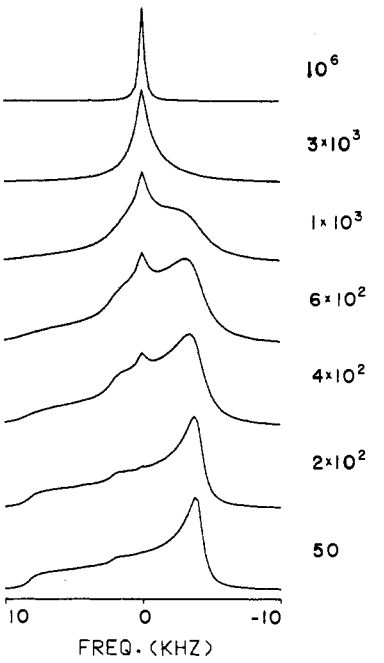

FIGURE 12: Theoretical computer simulations of chemical shift line shapes obtained with three-site hopping. The simulations were performed by using a model with the unique axis of the axially symmetric rigid lattice tensor oriented at the magic angle, 54.7° with respect to the diffusion axis. Rates on the right are in s^{-1}. The powder pattern is collapsed at hopping rates $>3 \times 10^3$ s^{-1}. Note that this discrete motion model results in spectra which are qualitatively similar to the experimental results for PC's and the lipid mixtures.

powder pattern. In summary, this model for the motion of the DPPE molecules, which involves an axially symmetric tensor tilted at the magic angle, and relies on the thermally activated axial diffusion rates going from slow to fast exchange to narrow the spectrum, is not consistent with the experimentally observed ^{2}H and ^{13}C results.

The second model which can be used to explain the narrowing of the DPPE ^{13}C spectra assumes that there is rapid long axis diffusion on the ^{13}C time scale in both the L_β and L_α phases; e.g., eq 2 is satisfied in both phases. The ^{2}H chain labeled spectra of Figure 1 indicate that the axial hopping rate must be $\sim 10^5$ s^{-1}, and this assumption is consistent with these results. Next we assume that in the L_β phase the unique axis of the ^{13}C tensor is oriented with respect to the diffusion axis such that it yields the observed $\Delta\sigma$ = 95 ppm pattern. Moreover, since the motion is fast, the features of this pattern are well delineated as are observed. For this case, the breadth of the motionally averaged tensor, $\Delta\sigma^R$, has been calculated and is (Mehring et al., 1971)

$$\Delta\sigma^R = [\sigma_{33} - \tfrac{1}{2}(\sigma_{11} + \sigma_{22})][\tfrac{1}{2}(3\cos^2\theta - 1)] + \tfrac{3}{4}(\sigma_{11} - \sigma_{22})\sin^2\theta\cos 2\phi \quad (4)$$

where the σ_{ii} values are the rigid lattice tensor elements and ϕ and θ are Euler angles which specify the tensor orientation relative to $\hat{D}$ (Rose, 1957). In the dry powder or in frozen aqueous dispersions at low temperatures, we observed a slightly axially asymmetric tensor for the lecithins and DPPE (see Table I) which means that a rigorous interpretation of our *sn*-2 ^{13}C spectra would require two Euler angles (ϕ and θ) to orient the tensor relative to $\hat{D}$. Since the powder spectra of, for example, Figure 2 provide a single number, $\Delta\sigma^R$, the problem is undetermined. However, inspection of the dry powder spectrum in Figure 4 and the rigid lattice principal values listed in Table I shows that the asymmetry in σ is small, amounting to about 15% of the total breadth. Moreover, a precise

Table I: Breadth of the L_β or $L_{\beta'}$ Axially Symmetric Powder Patterns for the Four Pure Lipids and the Width of the Isotropic Line in the L_α Phase at the Indicated Temperatures[a]

	L_β or $L_{\beta'}$ phase			L_α phase		
lipid	T (°C)	$\Delta\sigma$ (ppm)	θ (deg)[b]	T (°C)	$\Delta\sigma$ (ppm)	θ' (deg)
2-[1-^{13}C]DPPE	23	97	28	69	2	54.7
2-[1-^{13}C]DMPC	−5	110	24	29	3	54.7
1-[1-^{13}C]DMPC	−5	107	27	29	32	47
2-[1-^{13}C]DPPC	22	110	24	42	6.5	54.7
2-[1-^{13}C]DSPC	20	88	31	57	4	54.7
	σ_{11}	σ_{22}	σ_{33}			
lecithin dry powder	−134	−8	14			
DPPE/50% H_2O, −55 °C	−133	−13	11			

[a] θ indicates the angle between the unique tensor axis and D calculated from eq 5 by assuming an axially symmetric rigid lattice tensor with $\Delta\sigma^{RL}$ = 148 ppm for the PC's and $\Delta\sigma^{RL}$ = 144 ppm for DPPE. Principle values for the rigid lattice $^{13}C{=}O$ tensors (relative to C_6H_6) obtained from dry powders and frozen aqueous dispersions are also included. [b] Using the average value of σ_{22} and σ_{33} rather than σ_{33} in calculating $\Delta\sigma^{RL}$ results in θ changing by a few degrees. For example, for DSPC, θ would be 29° rather than 31°.

knowledge of the molecular orientation of this tensor, which is at the moment unavailable, together with, for example, orientation-dependent studies (Griffin et al., 1978) would only permit us to determine the orientation of the C=O moiety with respect to $\hat{D}$. Although this is interesting structural information, it is independent of the conclusions presented here. Therefore, for the remainder of the discussion, we assume that σ is axially symmetric with traceless principal values of $\sigma_\parallel$ = −96 and $\sigma_\perp$ = 48 ppm for DPPE. With this assumption, we can neglect the second term in eq 4 and obtain

$$\Delta\sigma^R = (\sigma_\parallel - \sigma_\perp)[\tfrac{1}{2}(3\cos^2\theta - 1)] \quad (5)$$

Using the values above for $\sigma_\parallel$ and $\sigma_\perp$ and $\Delta\sigma^R$ from Table I, we find $\theta \approx 28°$ for the L_β phase. The powder pattern collapses to an isotropic line $\Delta\sigma^R \simeq 0$ and θ = 54.7° upon passing through the phase transition. Thus, in the context of this interpretation, there must be a conformational change which shifts the $\sigma_\parallel$ axis of the tensor from ~28° to 54.7° with respect to the diffusion axis. The derivation of eq 5 assumes axially symmetric continuous or small angle jump diffusion which always results in an axially symmetric motionally averaged tensor. An identical spectrum would be observed if the motion involved large angle jumps, e.g., 120° jumps, so long as the motion has 3-fold or greater symmetry and the rate satisfies eq 2. This model provides a consistent interpretation of the ^2H and ^{13}C results in Figures 1 and 2, and we believe it is the correct model to employ in understanding the remaining ^{13}C spectra in this paper.

Lecithins. The ^{13}C spectra in Figures 3–5 of pure lecithins show that these phospholipids share some common features with the phosphatidylethanolamine spectra of Figure 2. For example, in the $L_{\beta'}$ phase, the axially symmetric spectrum characteristic of the gel state is observed, and this collapses to the narrow line in the L_α phase. There are, however, some differences in the details of the spectra as can be seen by examining Table I where the principal values of the dry powder shift tensors, the breadths of the gel phase powder patterns, and the widths of the L_α phase lines are compared. These small differences can be accounted for by assuming slightly different conformations at the *sn*-2 position for the four pure phospholipids. Thus, we have also included in this table the angles θ and θ' which were calculated from eq 5 by assuming axially symmetric rigid lattice spectra. These angles refer to the angle between the unique axis of the shielding tensor and the molecular diffusion axis in the L_β (and $L_{\beta'}$) phases and the L_α phases, respectively. The fact that the angle θ is roughly constant indicates that the conformation at the *sn*-2 carbonyl is very similar for all four lipids in their gel phases. Furthermore, the gel phase powder patterns all collapse to a narrow line of roughly constant width in the L_α phase. Thus, DPPE, DMPC, DPPC, and DSPC all undergo quite similar conformational changes at their respective main, first-order phase transitions. The fact that the conformation in the L_α phase is quite similar is not surprising, since, for example, the ^2H spectra of phospholipids labeled at the 2 position of the *sn*-2 chain all exhibit two overlapping quadrupole powder patterns with similar residual quadrupole couplings (Seelig & Browning, 1978). To date, a comparison between conformations or dynamic properties in the gel state has not been possible, and thus these results represent the first attempt to make this comparison.

Although there are similarities in the spectra shown in Figures 2–5, there are nevertheless easily discernible differences, and these are connected with the way in which the L_β or $L_{\beta'}$ powder patterns transform to the isotropic L_α line. In the case of DPPE (Figure 2), this transformation occurs precipitously at the main phase transition (T_c = 64 °C). However, for all three PC's, the collapse occurs gradually over a 5–15 °C temperature range. In the case of DMPC, the L_α line is first observed in the spectrum at 7 °C shown in Figure 3 and for DPPC it is initially apparent in the 27 °C spectrum of Figure 4, which are, respectively, 17 and 15 °C below the main phase transition temperatures of 23.9 and 41.4 °C (Chapman et al., 1967; Mabrey & Sturtevant, 1976). For DSPC, there is a hint of the L_α line in the 48 °C spectrum of Figure 5, and the T_c for this lipid is 54.9 °C (Chapman et al., 1967; Mabrey & Sturtevant, 1976). Note also that the L_α line grows in intensity at the expense of the $L_{\beta'}$ pattern with increasing temperature until there is a clear superposition of the two spectra a few degrees below the main transition temperature. This is most readily apparent in the DMPC and DPPC spectra of Figures 3 and 4.

It is well-known that lecithins undergo a pretransition at temperatures a few degrees below the main transition, and we believe the premature appearance of the L_α line, and subsequently of the superposition of the $L_{\beta'}$ and L_α spectra, is associated with this transition and the formation of the intermediate $P_{\beta'}$ phase (Janiak et al., 1976, 1979). There are several experimental observations which support this view. First, phosphatidylethanolamines do not exhibit a $P_{\beta'}$ phase (McIntosh, 1980), and correspondingly the superposition of the L_α and L_β patterns is not observed in the *sn*-2 carbonyl DPPE spectra of Figure 2. Second, at low H_2O contents (~20 wt %), PC's transform directly from the $L_{\beta'}$ to the L_α phase (Janiak et al., 1979), and ^{13}C spectra of such low H_2O DMPC samples indeed do not exhibit the two-component spectra shown in Figures 3–5 (R. J. Wittebort and R. G. Griffin, unpublished results). Third, the temperatures at which the L_α line first appears, and the temperature range over which the superposition of L_α and $L_{\beta'}$ patterns is observed, correlate nicely with the calorimetric data for the three types of lecithins investigated. In Table II we have assembled these data which consist of the pretransition and main transition temperatures, and the temperature range over which the $P_{\beta'}$ phase exists, together with the temperatures at which the L_α line is first observed. In addition, the temperature interval over which

Table II: Thermal and Spectroscopic Data for the Three Lecithins DMPC, DPPC, and DSPC[a]

	$T_{c'}$	T_c	$\Delta T_{P_{\beta'}}$	T_{L_α}	$\Delta T_{L_{\beta'}+L_\alpha}$
DMPC	14.2	23.9	9.7	7	17
DPPC	35.3	41.4	6.1	27	15
DSPC	51.5	54.4	3.4	48	7

[a] $T_{c'}$ is the pretransition temperature, T_c is the main transition temperature, and $\Delta T_{P_{\beta'}}$ is the temperature interval over which the $P_{\beta'}$ phase exists. T_{L_α} is the temperature at which the L_α-like line first appears in the *sn*-2 ^{13}C=O spectra, and $\Delta T_{L_{\beta'}+L_\alpha}$ is the temperature interval over which the superposition of the $L_{\beta'}$ and L_α patterns is observed. The data indicate the superposition is due to the presence of the $P_{\beta'}$ phase. All temperatures are given in °C.

the superposition of L_α and $L_{\beta'}$ patterns is seen is also tabulated. For DMPC and DPPC, the L_α-like line first appears about 7 °C below T_c, and the superposition is evident over about a 15 °C temperature range. For DSPC, the corresponding numbers are smaller—4 and 7 °C, respectively—as they should be, since the $P_{\beta'}$ region in this lipid is only 3.4 °C wide. In summary, there are three lines of experimental evidence which strongly suggest that the superposition of L_α and $L_{\beta'}$ patterns observed for *sn*-2 ^{13}C=O labeled lecithins is due to the presence of the $P_{\beta'}$ phase.

If this hypothesis is correct, then overlapped powder patterns should also be evident in the spectra of PC's labeled at other positions, and Figure 6 shows that this is indeed the case. In this figure are illustrated ^{1}H-decoupled ^{13}C spectra of 1-[1-^{13}C]DMPC as a function of temperature, and at low temperatures (−5 to +6 °C) an axially symmetric spectrum of 107-ppm breadth is seen. As the temperature is raised, the parallel edge of the C=O pattern broadens, and in the 9 °C spectrum a new perpendicular edge is evident. Its position, as well as the position of the initial perpendicular edge, is marked for clarity with dashed lines. As the temperature is increased further, the intensity of the new perpendicular component increases, and at 22 °C, it alone is seen. Note also that at temperatures above 22 °C the parallel edge of the pattern has regained its sharpness, and, for example, at 29 °C, a single well-defined powder pattern is evident. The peak at the isotropic resonance frequency is the *sn*-2 C=O line which is present because, as mentioned above, some chain migration occurred during the reacylation of the lyso-PC. Nevertheless, it is clear from Figure 6 that at temperatures corresponding to the $P_{\beta'}$ phase (14–24 °C) there are two overlapping powder patterns present in the *sn*-1 ^{13}C=O spectra. The breadths of the $L_{\beta'}$ and L_α *sn*-1 C=O spectra and the associated angles θ and θ' are listed in Table I. In the case of the *sn*-1 carbonyl, the change in the angle on passing through the phase transition is about 20°.[3]

We believe that the *sn*-2 carbonyl spectra shown in Figures 3–5 and the *sn*-1 carbonyl results of Figure 6 can best be explained by assuming the presence of at least two different conformations of PC molecules in the $P_{\beta'}$ phase. As was discussed previously (Wittebort et al., 1981) and above in connection with DPPE, a model which attributes the narrowing of the *sn*-2 spectra to increased rates of axial diffusion alone does not suffice to explain the results. A continuous diffusion model results in line shapes which are broadened and rounded instead of the sharp patterns that are observed experimentally. While a discrete motional model reproduces some of the features of the experimental results, albeit only qualitatively, it is inconsistent with the axial diffusion rates obtained from the ^{2}H spectra of 2-[4,4-$^2H_2$]DPPE shown in Figure 1. In particular, it would result in ^{13}C spectra with only the L_α-like line. However, if it is assumed that the axial motion in the L_β or $L_{\beta'}$ and L_α phases is fast on the ^{13}C time scale, then it is possible to arrive at a consistent interpretation of the spectra. In the low-temperature $L_{\beta'}$ phase, the axially symmetric tensor is oriented so that its unique axis is at an angle of ~28° with respect to the diffusion axis, whereas in the L_α phase it is at ~54°, the magic angle, and the powder pattern collapses. The observation of a superposition of these two patterns then leads to a model of the $P_{\beta'}$ phase in which two long-lived conformations are present in the rippled bilayer (Wittebort et al., 1981).

So far we have discussed the ^{13}C spectra of the $P_{\beta'}$ phase simply in terms of the presence of two conformations at the *sn*-2 carbonyl, and we have assumed that there is rapid axial diffusion about $\hat{D}$. However, if this were the only motion present, then the spectra would consist of a sharp L_α line superimposed on the $L_{\beta'}$ pattern. Inspection of the experimental spectra in Figures 3 and 4 shows that this is not the case. Instead, the L_α-like component seen in the spectra of the $P_{\beta'}$ phase is noticeably wider than the line observed above T_c. In addition, relaxation experiments reported previously for DPPC (Wittebort et al., 1981) show that T_2 in the $P_{\beta'}$ phase is short, 0.3 ms at T = 37 °C, whereas in the $L_{\beta'}$ and L_α phases T_2 is long, 1.6 ms at T = 20 °C, and 7.2 ms at T = 47 °C, respectively, and these observations suggest that there is chemical exchange between the two lipid conformations. It is well-known that lipid molecules are not fixed in the lattice but rather that there is extensive lateral diffusion in the bilayer plane. In the $L_{\beta'}$ phase of lecithins, diffusion constants of about 10^{-11}–10^{-10} cm^2/s have been observed, and these increase to about 10^{-8}–10^{-7} cm^2 s^{-1} in the L_α phase (Rubenstein et al., 1979; Smith & McConnell, 1978; Sheats & McConnell, 1978). The presence of such lateral diffusion would result in the L_α-like lipid molecules exchanging with those which are responsible for the $L_{\beta'}$ pattern, and as a result, both spectral components would be broadened. On the left of Figures 3–5, we showed computer simulations which account for this exchange, and we see that there is excellent agreement between the simulations and the experimental spectra. In performing these simulations, we have assumed a model which is basically a six-site chemical exchange model, the details of which will be described in a separate publication (R. J. Wittebort and R. G. Griffin, unpublished results). First, we assume two types of molecules with angles $\theta \approx 24°$ ($L_{\beta'}$) (see Table I) and θ' = 54.7° between $\hat{D}$ and the unique tensor axis, $\sigma_\parallel$, and both are allowed to execute rapid 3-fold jumps (10^6 s^{-1}) about $\hat{D}$. In addition, molecules with the $L_{\beta'}$ and L_α orientations are allowed to exchange. The fixed parameters that are incorporated into the simulations are then the rigid lattice tensor values, the angle θ', and the axial hopping rate. The fraction of molecules which contribute to the L_α line (f_{L_α}), the angle θ, and the exchange rate $L_{\beta'} \rightarrow L_\alpha$ are adjusted in order to simulate the spectra. The values of these parameters which were used for the simulations shown in Figures 3 and 4 are assembled in Table III. Inspection of this table shows that θ is about 24° at the low temperatures and increases slightly to about 30–32° at temperatures immediately below T_c. Although it was not absolutely necessary to let this angle vary with temperature in order to obtain reasonable facsimiles of

[3] Recently Cornell (1981) reported natural-abundance spectra of some lecithins, and the general spectral behavior is similar to that described here. However, the C=O groups of the two chains were not separately labeled, and thus it was not possible to, for example, assign the powder pattern seen in the L_α phase to the *sn*-1 chain.

Table III: Parameters Employed in the Computer Simulations of the *sn*-2 $^{13}C{=}O$ Spectra Shown in Figures 3 and 4 [a]

DMPC				DPPC			
T (°C)	f_{L_α}	$\theta_{L_{\beta'}}$ (deg)	k_{ex} (s^{-1})	T (°C)	f_{L_α}	$\theta_{L_{\beta'}}$ (deg)	k_{ex} (s^{-1})
−5	0.02	24	30	22	0.01	24	5
7	0.10	29	30	24	0.01	24	5
9	0.12	29	30	27	0.03	27	10
11	0.17	30	40	30	0.05	28	10
13	0.18	30	40	32	0.13	28	30
17	0.27	31	100	36	0.40	32	100
20	0.43	32	200	38	0.50	32	100
22	0.53	32	250	42	0.95	30	900
24	0.75	40	300				

[a] f_{L_α} is the fraction of lipid in the L_α form. $\theta_{L_{\beta'}}$ is the angle between the unique axis of the *sn*-2 $^{13}C{=}O$ tensor and the diffusion axis for the $L_{\beta'}$ form. The L_α form tensor was assumed to be at the magic angle, 54.7°. k_{ex} is the rate constant for exchange from the $L_{\beta'}$ to the L_α form.

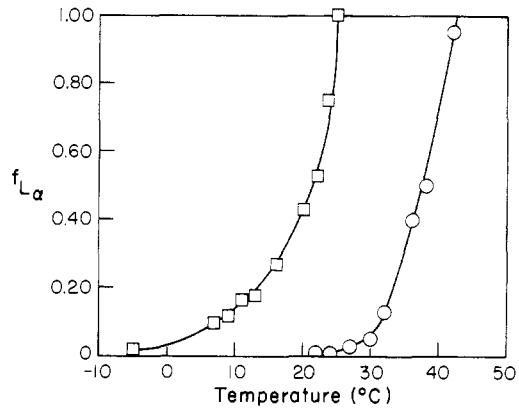

FIGURE 13: Plots of f_{L_α} vs. temperature for DMPC (□) and DPPC (○). The data were obtained from simulations shown in Figures 3 and 4 and are compiled in Table III.

the experimental results, we found that better simulations could be produced if it did change slightly. The change in this angle may reflect the fact that the $L_{\beta'}$-like portion of the bilayer is expanding slightly, and as a consequence, the amplitudes of the molecular fluctuations around $\hat{D}$ are increasing with temperature. Alternatively, fluctuations in the angle between the unique tensor axis and $\hat{D}$ might explain this variation. A similar size change in "tilt angle" has been reported by Janiak et al. (1976). Nevertheless, the angle is roughly constant and thus indicates that the molecules in the bilayer which contribute to the $L_{\beta'}$ component are structurally quite similar to those found in the pure $L_{\beta'}$ phase.

As the temperature is increased, f_{L_α} increases and k_{ex} increases as expected, and f_{L_α} data are plotted in Figure 13 for both DMPC and DPPC as a function of temperature. The shapes of these curves are similar for both lipids and show a slight positive slope until about 7 °C below T_c. At this point, the slope increases rapidly with further increases in temperature. It is interesting that f_{L_α} is about 0.3 for each lipid at the temperature corresponding to the peak of the pretransition endotherm and increases to about 0.5 at the midpoint between the pretransition and main transition temperatures. These similarities, plus the similarities in the shapes of the two curves, indicate that the mechanism of the pretransition—e.g., the manner in which the rippled phase is formed—is probably quite similar for DMPC and DPPC.

In X-ray studies of lecithins, it was reported that the ripple spacing—e.g., the 01 reflection—was first apparent at the peak of the pretransition endotherm. The curves of Figure 13 may partially explain why this is the case even though the bilayer exhibits some L_α character well before the pretransition. In particular, the ^{13}C NMR experiment shows that at the peak of the endotherm the fraction of L_α molecules is still only about 30% and thus the ripple reflections were probably not strong enough to detect prior to this point.

The k_{ex} vs. T data of Table III also show that the exchange rate increases rapidly once the $P_{\beta'}$ phase is present. For example, at temperatures slightly below the pretransition temperature (7 °C for DMPC and 27 °C for DPPC), we obtain numbers for k_{ex} of 10–30 s^{-1}, but midway between the pretransition and main transition, this number has increased by approximately an order of magnitude. This behavior is consistent with measurements of the diffusion constants determined from photobleaching experiments (Smith & McConnell, 1978; Rubenstein et al., 1979) as the following considerations will show.

The relation between the translational diffusion coefficient, D_T, and the mean square displacement, $\overline{x^2}$, in a time t for diffusion in two dimensions is (Saffman & Delbrück, 1975)

$$\overline{x^2} = 4D_T t \qquad (6)$$

Rubenstein et al. (1979) reported a diffusion coefficient of $\sim 7 \times 10^{-11}$ cm^2 s^{-1} for DMPC at 16 °C. At this particular temperature, we find k_{ex} values of ca. 200 s^{-1}. Associating k_{ex} with $1/t$ and inserting these values into eq 6, we find $(\overline{x^2})^{1/2} \approx 120$ Å. Thus, we calculate that in 5×10^{-3} s a liquid molecule diffuses ~120 Å in passing from an L_α-like "domain" to an $L_{\beta'}$-like "domain". If we assume that these two domains correspond to particular regions in the bilayer ripple profile, then $(\overline{x^2})^{1/2}$ would be approximately half the ripple period, which is ~75 Å for DMPC (Janiak et al., 1976). Thus, with this assumption, the calculated exchange rate constants are qualitatively consistent with the reported diffusion coefficients. One must keep in mind, however, that lateral diffusion in a rippled bilayer may well be anisotropic; i.e., the coefficients for diffusion parallel and perpendicular to the ripples may be different (Owicki & McConnell, 1980). In this case, the reported D_T values are some kind of average value, and a comparison with our k_{ex} values is even more difficult. The diffusion coefficient in the $P_{\beta'}$ phase is strongly temperature dependent and for DMPC increases by about an order of magnitude between 10 and 20 °C (Rubenstein et al., 1979). If the average distance between the two exchanging lipid components does not change, then the k_{ex} values should be directly proportional to the diffusion coefficient. Indeed, qualitatively we observe an increase of k_{ex} by about an order of magnitude in this particular temperature range. However, a direct quantitative comparison between D_T and k_{ex} is not possible at the present time because the interpretation of the k_{ex} values obviously depends on the underlying model for the rippled phase.

In summary, our ^{13}C NMR results on pure lecithins show that formation of the $P_{\beta'}$ phase results in the appearance of lipid molecules with two long-lived conformations in the *sn*-1 and *sn*-2 carbonyl regions of the molecule. The conformations appear to be quite similar to those seen in the low- and high-temperature $L_{\beta'}$ and L_α phases, at least in the carbonyls, and may be related to the conformations recently found in crystals of DMPC obtained from ether/ethanol/H_2O (Pearson & Pascher, 1979). Furthermore, the fraction of the L_α-like molecules grows with increasing temperature, and, because of lateral diffusion in the bilayer, there is a temperature-dependent chemical exchange between the two forms. In view

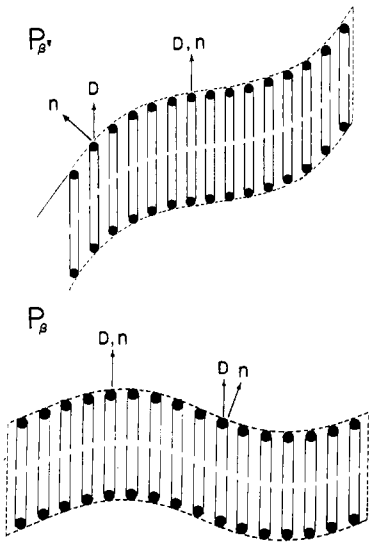

FIGURE 14: Two schematic representations of the monoclinic phase of lecithins: (top) $P_{\beta'}$ model where $\langle\beta\rangle \neq 0$, and (bottom) P_β model where $\langle\beta\rangle = 0$. Note that both models contain regions where $\hat{n}$, the bilayer normal, is parallel to $\hat{D}$, the molecular long axis, as well as regions where $\hat{D}$ is tilted with respect to $\hat{n}$. It is possible that this locally varying tilt leads to the coexistence of the L_α and $L_{\beta'}$ ^{13}C spectra of lecithins shown in Figures 3–5.

of these results, one can speculate on a model of the $P_{\beta'}$ phase which incorporates these features as well as features found in other experiments.

The macroscopic structure of the monoclinic phase has been investigated extensively with X-ray diffraction (Tardieu et al., 1973; Janiak et al., 1976, 1979; Stamatoff et al., 1981) and with electron microscopy (Luna & McConnell, 1977), and it is generally agreed that the phase is rippled. However, the X-ray studies disagree as to how the chains are tilted. For example, Janiak et al. (1976, 1979) favor a $P_{\beta'}$ model in which there is a nonzero average tilt which varies locally along the ripple profile as is shown in Figure 14 (top). In contrast, Stamatoff et al. (1981) have suggested that the average tilt angle is zero—e.g., that the chains are all perpendicular to the average bilayer plane, a P_β model—but that the tilt angle locally departs from zero [Figure 14 (bottom)]. A third model, involving folded bilayers, has been described by Larsson (1977), and in this case, the ripple consists of regions of tilted ($L_{\beta'}$-like) and untilted (L_β-like) lipid chains. Finally, Meier et al. (1982) have described a fourth alternative, based on biradical ESR spectra, where all the lipid molecules are parallel to the local bilayer normal. Other X-ray experiments by Brady & Fein (1977) and Graddick et al. (1979) indicate that the acyl chains assume some liquid-crystalline-like properties in the pretransition region, and similar conclusions have been drawn from Raman spectroscopy (Levin & Bush, 1981; Vogel & Jähnig, 1981), infrared investigations (Cameron et al., 1981a,b), and dilatometry (Nagle, 1973; Nagle & Wilkinson, 1978). Similarly, ^{31}P NMR studies of the head group (Campbell et al., 1979) and ESR saturation transfer experiments (Marsh, 1980) detect shorter correlation times in the monoclinic phase, and ^{2}H NMR experiments on DPPC with perdeuterated acyl chains (Davis, 1979) show that the second moment of the spectrum decreases in the pretransition region. The decrease is again indicative of additional motional averaging. ^{2}H NMR spectra of specifically ^{2}H labeled lecithins obtained in this laboratory show no precipitous changes in the pretransition region. Nevertheless, when compared to spectra of the $L_{\beta'}$ phase, there are notable differences. For example, chain-labeled spectra show what appear to be at least two components, and similar multicomponent spectra are observed for glycerol backbone and head group labeled molecules. In summary then, it is agreed that the phase in the region between the calorimetric pretransition and main transition is rippled and that it exhibits some L_α as well as $L_{\beta'}$ character.

The ^{13}C spectra of Figures 3–5 make it clear that the L_α fraction appears at temperatures well below the peak of the pretransition endotherm and that it grows at the expense of the $L_{\beta'}$ fraction until the main phase transition is reached. This picture is somewhat different from that derived from X-ray studies where it is presumed that the $P_{\beta'}$ phase is formed at the peak of the pretransition and is essentially static in character thereafter. For example, in the data of Janiak et al. (1976, 1979), the 01 spacing due to the ripple is observed to be temperature independent. If this is the case, then other features of the ripple structure may be changing, for example, the amplitude, and this would lead to the increase in the intensity of the L_α line in our ^{13}C spectra. This is a point which obviously requires further investigation.

In addition, the spectra of Figures 3–5 indicate the presence of two long-lived conformations in this phase, that there is exchange between these fractions, and that the exchange constants are consistent with a separation of $\sim$100 Å. This observation suggests that the L_α and $L_{\beta'}$ fractions occupy different portions of the ripple profile, and the representations of Figure 14 suggest one way in which this structural and perhaps dynamical inequivalence could be accommodated.

The two structures shown in Figure 14 differ in that the average tilt angle, $\langle\beta\rangle$, with respect to the bilayer plane is nonzero in the $P_{\beta'}$ model whereas in the P_β model $\langle\beta\rangle = 0$. However, both structures exhibit the feature that the local tilt angle, β_L, varies along the ripple profile and $\beta_L \approx 0$ in some regions, e.g., where $\hat{D}$, the molecular long axis, is parallel to $\hat{n}$, the local bilayer normal, as shown. Similar statements are applicable to the folded bilayer model of Larsson (1977). An undisputed structural difference between the $L_{\beta'}$ and L_α phases of lecithins is the difference in tilt angle with respect to the bilayer normal. In the L_α phase, $\beta = 0$, whereas in the fully hydrated $L_{\beta'}$ phase $\beta \simeq 30°$. Both of the rippled structures in Figure 14 contain regions which exhibit these tilt angles, and it is possibly this feature which leads to the coexistence of the L_α and $L_{\beta'}$ patterns in our ^{13}C NMR spectra. Specifically, in regions of the profile where $\beta \approx 0$, the bilayer is locally flat. Thus, in these regions, the microscopic structural constraints necessary for the conformational change at the *sn*-2 carbonyl could be satisfied, and thus they give rise to the L_α line. Correspondingly, those regions where $\beta_L \neq 0$ would yield the $L_{\beta'}$ ^{13}C pattern. It is also possible that the increased chain disorder observed in the Raman, infrared, and X-ray experiments could be accommodated by the untilted portions of the ripple. We emphasize that things other than, or in addition to, local tilt may control the mechanism of the conformational change which we observe at the *sn*-2 carbonyl; thus, the discussion above is subject to further experimental refinement. *Nevertheless, the experimental results of Figures 3–5 offer compelling evidence that the ripple phase is structurally heterogeneous and that a locally varying structure is an essential microscopic feature of this phase of lecithins.*[4]

Phospholipid/Cholesterol Mixtures. It is well-known that CHOL has dramatic effects on the phase behavior of lipid bilayers. The most well-documented and discussed example

[4] Some theoretical discussions of the ripple phase have been published (Gebhardt et al., 1977; Doniach, 1979; Chan & Webb, 1981), and a recent one (Falkowitz et al., 1982) predicts the $P_{\beta'}$ phase to be structurally heterogeneous as suggested here.

Table IV: Parameters Employed in the Computer Simulations of the *sn*-2 $^{13}C{=}O$ Spectra Shown in Figures 7, 9, and 10[a]

DPPE/20% CHOL				DPPC/30% CHOL				DSPC/30% CHOL			
T (°C)	f_{L_α}	θ (deg)	k_{ex} (s^{-1})	T (°C)	f_{L_α}	θ (deg)	k_{ex} (s^{-1})	T (°C)	f_{L_α}	θ (deg)	k_{ex} (s^{-1})
1	0.1	28	2×10^2	−10	0	33	0	0	0.04	31	30
11	0.18	28	3×10^2	−5	0.09	33	5×10^2	10	0.08	33	70
23	0.30	28	4×10^2	0	0.28	33	5×10^2	20	0.25	33	2.7×10^2
34	0.48	28	5×10^2	5	0.40	35	8×10^2	30	0.45	36	4.9×10^2
45	0.80	28	7×10^2	10	0.50	40	10^3	40	0.65	40	5.6×10^2
55	1.00	28	10^3	20	0.80	40	10^3	50	1.00		
				30	1.00						

[a] An explanation of the parameters is given in Table III. In the DPPE/20% CHOL spectra, the angle θ was fixed at 28°, whereas for the lecithin/CHOL samples it was allowed to vary as shown.

of this phenomenon is probably the abolition of the sharp component in the DSC endotherm of lecithins at CHOL concentrations greater than about 20 mol %. Therefore, it is of interest to determine the effect of CHOL on the *sn*-2 $^{13}C{=}O$ spectra, and accordingly, we have recorded spectra of phospholipid/CHOL mixtures. Some results for selected CHOL concentrations are shown in Figures 7–10 for DPPE, DMPC, DPPC, and DSPC, respectively. We have chosen these results to illustrate the following three points. First, CHOL induces the appearance of the sharp L_α-like line, and it alone is seen at high CHOL concentrations well below the transition temperature of the pure lipids. This is the case for all four lipids studied. Second, the phase transition mechanism in the presence of CHOL is clearly different from that seen in pure DPPE or in binary DPPC/DPPE mixtures but appears to be related to the mechanism observed in pure lecithins. Specifically, in the former two cases the conformational change at the *sn*-2 C=O occurs at the same temperatures at which the acyl chains disorder. However, in the presence of CHOL, the conformational change occurs at temperatures below those at which the chains exhibit sharp axially symmetric powder patterns. Third, a comparison of *sn*-2 $^{13}C{=}O$ spectra of the four lipids studied shows that CHOL interacts differently with different lecithins and differently with PE and PC. Finally, we discuss and compare results from DSC and NMR experiments for each CHOL/lipid mixture studied.

In the case of pure DPPE, the *sn*-2 $^{13}C{=}O$ spectra collapsed at T_c to a narrow line (see Figure 2). In the presence of 20 mol % CHOL, very different behavior is observed as is illustrated in Figure 7. Here the L_α line first appears at ~11 °C which is 53 °C below the T_c of pure DPPE, and a clear superposition of the L_α and L_β patterns is apparent in the interval from 11 to about 55 °C. The spectra can be simulated with the six-site exchange program, and the results are shown on the left of the figure. The data used for the simulations are assembled in Table IV, and f_{L_α} is plotted as a function of temperature in Figure 15 for DPPE/20 mol % CHOL. f_{L_α} is nearly linear in temperature and shows the coexistence of the two conformations over a wide temperature range. The k_{ex} data are similar to those obtained for pure lecithins—e.g., the rate constants are ~10^2 s^{-1}.

DSC investigations of DPPE/CHOL mixtures (Blume, 1980) show that addition of CHOL to PE results in a considerable broadening of the phase transition, and at CHOL concentrations greater than 30%, the endotherm is shifted to lower temperatures. With further increases in CHOL concentration, it eventually disappears into the base line. However, at 20 mol %, the onset of melting occurs at about 30 °C, and the trace is strongly asymmetric with a sharp peak which is roughly unshifted from the peak temperature observed for pure DPPE, e.g., 61 °C as opposed to 64 °C. In Figure 7, we see that the L_α-like line first appears in the 11 °C spectrum,

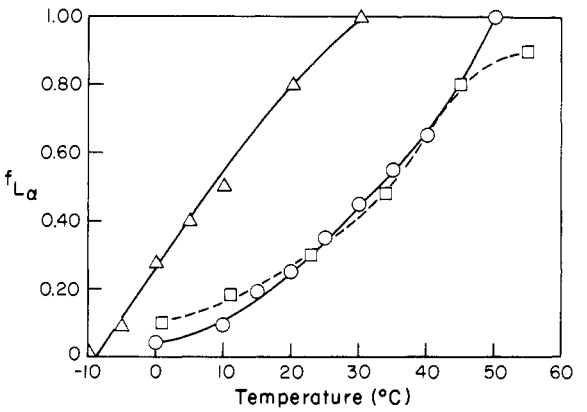

FIGURE 15: Plots of f_{L_α} vs. temperature for DPPE/20 mol % CHOL (□), DPPC/30 mol % CHOL (△), and DSPC/30 mol % CHOL (○).

which is about 20 °C below the onset of melting. The apparent discrepancy between the onset of melting and the first appearance of the L_α line in the ^{13}C NMR spectra can be reconciled if it is remembered that in a DSC experiment only the change in the apparent heat capacity due to a cooperative transition is usually detected. Any noncooperative change leads only to a slightly sloped base line which might escape observation. In contrast, alterations in the ^{13}C NMR spectra are due to variations in structural or dynamical properties at particular points in the lipid molecule, and these will be apparent even if they are not of a cooperative nature. Thus, the appearance of an L_α line ~20 °C below the onset of melting may only mean that at this temperature some of the lipid molecules are disordered (giving an L_α line) due to the presence of nearby CHOL molecules and that the fraction of disturbed lipids changes in a noncooperative fashion below the calorimetrically observed endotherm.

The sharp component of the endotherm, which occurs above 45 °C, cannot be associated with the conformational change at the *sn*-2 C=O, since the L_β powder pattern has collapsed to the narrow line at these temperatures. Rather, it appears that it is connected with disordering of the acyl chains and increased rates of axial and lateral diffusion. In particular, at 45 °C the spectrum of 2-[4,4-$^2H_2$]DPPE/20 mol % CHOL is a broadened axially symmetric powder pattern with $\Delta\nu_{Q\perp}$ = 52 kHz. This spectral line shape and splitting suggest that the chains are undergoing axial diffusion at rates of ~10^6 s^{-1}, and they are predominantly in an all-trans conformation. At temperatures above 45 °C, which corresponds to the onset of the sharp component, the splitting begins to decrease rapidly to a value of about 37 kHz at 68 °C. In addition, the spectral line shape sharpens. These are the types of changes expected if additional gauche isomers are forming, and if the axial diffusion rates and the lateral diffusion rates are increasing. Thus, the sharp component of the endotherm observed at 20

mol % CHOL can be associated with these effects, and therefore may indicate a gradual transformation to a pure L_α-like phase.

The spectra of the DMPC/CHOL mixture, in this case 25 mol % CHOL, shown in Figure 8 are also quite different from the spectra seen for the pure lipid. In the case of pure DMPC (Figure 3), the axially symmetric powder pattern is seen at temperatures up to 7 °C where the L_α line appears. The spectrum then gradually collapses to the L_α line with increasing temperature. In contrast, the addition of 25 mol % CHOL serves to induce the appearance of the L_α line over the entire temperature range as is shown in Figure 8. Because we are in the approximately pure L_α spectrum region, we have not included simulations of these spectra. However, for production of these results, the exchange rates must be $\sim 10^3$ s^{-1} and the portion of L_α-like molecules must always be greater than 0.7. At lower CHOL concentrations, the superposition of $L_{\beta'}$ and L_α patterns can be seen, and at sufficiently low temperatures, only the $L_{\beta'}$ pattern is observed.

As determined by DSC, the addition of CHOL to DMPC leads to an asymmetric broadening of the endotherm to higher temperatures. At concentrations greater than 20%, the sharp component has vanished, and what remains is a very wide heat absorption curve (Mabrey et al., 1978). Based on our discussion of the DPPE/CHOL system, we would expect in this case to see only the L_α-like line, and this is exactly what is observed in Figure 8. Finally, Rubenstein et al. (1979) have measured lateral diffusion coefficients with photobleaching techniques, and at these temperatures and CHOL concentrations, D_T is always greater than 10^{-9} cm^2/s, which should lead to fast exchange spectra.

The effect of 30 mol % CHOL on the ^{13}C spectra of 2-[1-^{13}C]DPPC and 2-[1-^{13}C]DSPC is illustrated in Figures 9 and 10, and the spectra bear some similarities to those observed for DPPE and DMPC/CHOL systems. For example, in the case of DPPC, the L_α line is seen at temperatures below the main transition temperature of the pure lipid as was observed for DPPE. DSPC behaves similarly although the effect is not as large since there is only a $\sim$10–15 °C lowering of the temperature at which the spectrum assumes almost complete L_α character. For example, the 40 °C spectrum still shows a remnant of the $L_{\beta'}$ pattern. A notable difference between the spectra of DPPE and DSPC/CHOL and DPPC/CHOL mixtures is the width of the L_α line. In DPPE and DSPC/CHOL, both the $L_{\beta'}$ or L_β and the L_α components are sharp when they coexist, and the measured exchange rates are relatively slow [$(1–5) \times 10^2$ s^{-1}]. However, in the case of DPPC at temperatures between 0 and 20 °C, the $L_{\beta'}$ pattern is present but noticeably broadened—e.g., in the 5 and 10 °C spectra of Figure 9, the line shape is nearly triangular, and at temperatures above $\sim$20 °C, only the L_α line is seen. The explanation of this effect is of course that at these CHOL concentrations and temperatures the exchange rate is larger, and inspection of the data in Table IV shows that this is indeed the case. For instance, with $f_{L_\alpha} \simeq 0.5$, $k_{ex} = 5 \times 10^2$ s^{-1} for DPPE/20% CHOL and DSPC/30% CHOL whereas for DPPC/30% CHOL $k_{ex} = 10^3$. Note also that for a given temperature f_{L_α} is much larger for DPPC/CHOL than for the other two lipid/CHOL mixtures. Inspection of Figure 15 shows for example that at 20 °C $f_{L_\alpha} = 0.8$ for DPPC/CHOL whereas for DPPE and DSPC $f_{L_\alpha} \simeq 0.25$–0.30. Finally, the plots in Figure 15 illustrate that 20% CHOL has almost the same effect on DPPE as does 30% CHOL on DSPC. In particular, the f_{L_α} vs. temperature plots for these two lipid/CHOL mixtures are very nearly identical. These similarities are also apparent in the k_{ex} data of Table IV and the line shapes of Figures 8 and 10.

The calorimetric behavior of DSPC/CHOL mixtures has not been investigated so in this case no comparisons with the NMR results are possible. Mabrey et al. (1978) and Estep et al. (1978) have investigated the DPPC/CHOL system calorimetrically, and Rubenstein et al. (1979) have studied it with photobleaching techniques. Both of the calorimetric investigations show that the addition of CHOL to DPPC results in the development of a broad component in the endotherm which increases in intensity up to about 25 mol % CHOL. Concurrently, the sharp component normally associated with the gel–liquid-crystalline transition decreases in intensity, and at 22–25% CHOL, it disappears. Thus, at 30 mol %, only a broad component with a peak maximum at about 45 °C and a transition enthalpy of 2.6 kcal/mol (Estep et al., 1978) is observed. The onset of this curve is at about 10 °C (Mabrey et al., 1978) and corresponds to the presence of a large L_α fraction in our ^{13}C NMR spectra. The shapes of the DSC endotherms for DPPC/30% CHOL and DMPC/20 mol % CHOL are quite similar, and correspondingly the NMR spectra are similar. For example, in both systems, the L_α line is seen about 20 °C below the transition temperature of the pure lipid, and well before the peak of the endotherm, the ^{13}C spectra assume almost total L_α character.

In summary, addition of CHOL to all four lipids results in the collapse of the L_β or $L_{\beta'}$ pattern to the L_α-like line at temperatures well below the transition temperature of the pure lipid bilayer. In addition, the DPPE/CHOL spectra suggest that CHOL alters the mechanism by which PE molecules transform from gel to liquid-crystalline behavior. In particular, the *sn*-2 C=O conformational change occurs first, and this is followed at higher temperatures by a disordering of the acyl chains. Thus, the broad component in the DPPE/CHOL DSC endotherm appears to be associated with the conformational change, and the sharp component with the disordering of the acyl chains. As outlined above, the general features of this phase transition mechanism are also observed in pure lecithins, and it is different from the mechanism observed in pure DPPE bilayers. Finally, it is clear from the discussion above that CHOL interacts differently with the three lecithins studied and differently with PE and PC.

Binary Phospholipid Mixtures. The final set of ^{13}C spectra we wish to discuss are those of the equimolar mixtures of DPPC/DPPE shown in Figure 11. Our purpose in investigating this system was to determine if the *sn*-2 ^{13}C=O spectra could be employed to detect the coexistence of gel and liquid-crystalline phases in this type of lipid mixture, and the spectra of Figure 11 indicate that this is the case. The spectra of a 2-[1-^{13}C]DPPC/DPPE mixture are shown on the left of Figure 11, and the axially symmetric gel phase spectrum is observed up to 45 °C where a hint of the L_α line is first apparent. In contrast, the spectrum of the DPPC/2-[1-^{13}C]DPPE mixture at this temperature shows only the L_β spectrum. However, since DPPE is the higher melting lipid, this is the expected behavior. A 5 °C increase in temperature to 50 °C results in the clear observation that the L_α component is more intense in the DPPC than in the DPPE spectrum. At 53 °C, the intensity of the L_β pattern is decreased substantially, and finally at 55 °C, only the L_α line is seen.

The phase behavior of these two lipids has been investigated by different methods, and it was concluded that they exhibit almost ideal miscibility over the entire composition range (Shimshick & McConnell, 1973; Blume & Ackermann, 1974; Lee, 1975; Mendelsohn & Koch, 1980). In addition, the phase

diagram is reasonably well established, at least in the equimolar region, and thus we can compare our results with these methods. The ESR spin-label data (Shimshick & McConnell, 1973) indicate phase boundaries at 48 and 56 °C, the regions below and above these temperatures corresponding to L_β and L_α phases. Between 48 and 56 °C, a two-phase region was postulated, presumably a mixture of L_β and L_α phases. Similar results were obtained with DSC (Blume & Ackermann, 1974), the fluorescent probe chlorophyll (Lee, 1975), and Raman spectroscopy (Mendelsohn & Koch, 1980). Our ^{13}C spectra for equimolar mixtures of DPPC and DPPE agree well with these results in that the L_α line is first seen at 45 °C in the DPPC spectra and the transition to the L_α phase is complete in both sets of spectra at 55 °C. Moreover, a coexistence of L_β and L_α spectra is clearly apparent in the spectra obtained between these temperatures.

On a molecular scale, the transition across these boundaries corresponds to a conformation change at the *sn*-2 carbonyl which alters the orientation of the ^{13}C tensor relative to the molecular diffusion axis. As a result, it is tempting to label the two types of molecules in this intermediate temperature range L_β and L_α. Theoretically, it should be possible to calculate the composition of the liquid-crystalline and gel phases—i.e., the tie lines in the phase diagram—by simulating the experimental spectra with the six-site exchange program mentioned above. However, the fits obtained by assuming a single exchange rate between the L_α and L_β ($L_{\beta'}$) components are not satisfactory. Instead, we have found it necessary to introduce a distribution of exchange rates, and we believe this may reflect the presence of a distribution of domain sizes in these mixtures. Another interesting point concerning the spectra of Figure 11 is that when the superposition of the L_β and L_α spectra are observed, the L_α line is noticeably narrower than in either pure PC bilayers or mixtures of PC or PE with CHOL. This can be easily seen by comparing the spectra of Figure 11 with the spectra shown in the Figures 3–10. This observation requires that exchange between the $L_{\beta'}$- and L_α-like domains in DPPC/DPPE mixtures be considerably slower than is observed in the other systems we have investigated. This suggests that the mixed bilayer $L_{\beta'}$-like lattice is reasonably well packed and is not disrupted so easily as is, for example, the PE or PC/CHOL lattice. As a result, the diffusion coefficient is low, and/or the domains in the transition region are much larger than in mixtures with cholesterol.

Finally, we should mention that when the L_α-like line is seen in the *sn*-2 $^{13}C{=}O$ spectra of DPPC/DPPE mixtures a sharp component is also observed in the ^2H spectra of chain-labeled DPPC or DPPE. This again indicates that exchange is slow and also that the phase transition mechanism is different in this case. For example, in the PE/CHOL mixtures discussed above, the conformational change at the *sn*-2 C=O was complete before the chains disordered. In this case, however, both of the molecular events happen at roughly the same temperatures. Nevertheless, it is clear from the results presented here that the conformational change at the *sn*-2 carbonyl, which can be induced thermally in pure PC's and PE's or by addition of CHOL, is also a characteristic of phase transitions in mixed phospholipid bilayers.

Conclusions

In a previous paper, we observed that the *sn*-2 $^{13}C{=}O$ spectra of DPPC transform from an axially symmetric powder pattern in the $L_{\beta'}$ phase to an isotropic line in the L_α phase, while in the intermediate $P_{\beta'}$ phase a superposition of the spectra was observed. This experiment provided the motivation for the investigations reported here, which was in general terms to determine if similar types of spectral effects are exhibited by other phospholipids. If so, then we wished to determine unambiguously the origin of the effect, and in addition to determine if it carries over into binary lipid mixtures.

Accordingly, we have reported here the temperature dependence of the $^{13}C{=}O$ spectra of DPPE and three lecithins—DMPC, DPPC, and DSPC—and as we have seen above, each of these lipids does indeed exhibit this effect. The DPPE *sn*-2 $^{13}C{=}O$ spectra, together with results from studies of ^2H-labeled DPPE, demonstrate unambiguously that the collapse of the axially symmetric powder pattern to the isotropic line is due to a conformational change at the *sn*-2 carbonyl which is associated with the $L_\beta \rightarrow L_\alpha$ phase transition. $^{13}C{=}O$ spectra of pure lecithins exhibit similar effects, and together these results suggest that this conformational change may be a common feature of phospholipid phase transitions. Moreover, the results emphasize the differences in the mechanisms of the phase transitions in the two classes of lipids. In the case of PE's, the transition occurs precipitously, whereas for lecithins some L_α character is present at temperatures well below the main transition temperature and even below the pretransition. It would clearly be of interest to pursue these experiments in other types of glycerol phospholipids such as phosphatidylserine and phosphatidylglycerol. Furthermore, we have demonstrated that the line shapes observed in the lecithin $P_{\beta'}$ phases can be satisfactorily explained by assuming chemical exchange (lateral diffusion) between the $L_{\beta'}$- and the L_α-like conformations. With the assumption that the effective domain separation is comparable to the ripple profile, then the exchange rate constants obtained are in good agreement with diffusion constants measured by other methods. These results lead to a model of the $P_{\beta'}$ phase with a locally varying microscopic structure.

Since the conformational change at the *sn*-2 carbonyl appears to be a common feature of pure phospholipid phase transition, we have extended these experiments to studies of phase transitions and phase equilibria in binary lipid mixtures. The addition of CHOL to DPPE results in a broad temperature region, ~40 °C, in which the superposition of the $L_{\beta'}$- and L_α-like spectra are observed. Again, the spectral line shapes indicate exchange between the conformations at rates which are similar to those observed for pure lecithins. The *sn*-2 $^{13}C{=}O$ spectra of lecithin/CHOL mixtures are both similar and different. In the case of DMPC, 25% CHOL is sufficient to produce almost complete L_α-type lipid for $T >$ 0 °C, whereas both DPPC and DSPC exhibit the superposition spectra over a finite range of temperatures at even higher CHOL concentrations. While this behavior is undoubtedly due in part to the different main transition temperatures of these lipids, the results also suggest that CHOL interacts differently with different lecithins. Since the results presented here indicate that this point is amenable to investigation with $^{13}C{=}O$ spectra, we intend to pursue it further in a future publication.

The remaining lipid mixture investigated was DPPC/DPPE, and again the results suggest that phase transitions and phase equilibria in this type of system can be studied with $^{13}C{=}O$ spectra. The spectra clearly indicate that coexisting phases can be observed, and it is possible to determine the position of phase boundaries by observing the appearance of the L_α line and the disappearance of the L_β pattern. In contrast to the spectra of the mixtures containing CHOL, the L_α component observed in the superposition spectra is sharp, indicating that exchange is slow.

In summary, it appears that the ^{13}C NMR spectra of the *sn*-2 carbonyl of phospholipids can be usefully employed to investigate a variety of phenomena in phospholipid bilayers. While we have confined our attention here to pure lipid bilayers and some lipid mixtures, the technique could obviously be utilized in investigations of the effect of other agents such as antibiotics on the structure of bilayer membranes and to studies of lipid/protein interactions. The single disadvantage of the approach is that it is confined to a single molecular position in the lipid molecule. Nevertheless, the results above suggest that this is an important molecular position when phase transitions and equilibria are involved, and the same may be true in other cases as well.

References

Bansil, R., Day, J., Meadows, M., Rice, D., & Oldfield, E. (1980) *Biochemistry 19*, 1938.

Bloom, M., Davis, J. H., & Valic, M. I. (1980) *Can. J. Phys. 58*, 1510.

Blume, A. (1980) *Biochemistry 19*, 4908.

Blume, A., & Ackermann, T. (1974) *FEBS Lett. 63*, 71.

Blume, A., Wittebort, R. J., Das Gupta, S. K., & Griffin, R. G. (1982) *Biochemistry* (in press).

Boss, W. F., Valley, C. J., & Landsberger, F. R. (1975) *Anal. Biochem. 64*, 289.

Brady, G. W., & Fein, D. B. (1977) *Biochim. Biophys. Acta 466*, 249.

Büldt, G., Gally, H. V., Seelig, J., & Zaccai, G. (1979) *Biochemistry 20*, 4496.

Cameron, D. G., Gudgin, E. F., & Mantsch, H. H. (1981a) *Biochemistry 20*, 4496.

Cameron, D. G., Casal, H. L., Mantsch, H. H., Boulanger, Y., & Smith, I. C. P. (1981b) *Biophys. J. 34*, 1.

Campbell, R. F., Meirovitch, E., & Freed, J. H. (1979) *J. Phys. Chem. 83*, 525.

Chakrabarti, P., & Khorana, H. G. (1975) *Biochemistry 14*, 8021.

Chan, W. K., & Webb, W. B. (1981) *Phys. Rev. Lett. 46*, 39.

Chapman, D., Williams, R. M., & Ladbrooke, B. D. (1967) *Chem. Phys. Lipids 1*, 445.

Cornell, B. (1981) *Chem. Phys. Lipids 28*, 69.

Das Gupta, S., Rice, D., & Griffin, R. G. (1982) *J. Lipid Res. 23*, 197.

Davis, J. (1979) *Biophys. J. 27*, 339.

Davis, J. H., Jeffrey, K. R., Bloom, M., Valic, M. I., & Higgs, T. P. (1976) *Chem. Phys. Lett. 42*, 390.

Doniach, S. (1979) *J. Chem. Phys. 70*, 4587.

Estep, T. N., Mountcastle, D. B., Biltonen, R. C., & Thompson, T. E. (1978) *Biochemistry 17*, 1974.

Falkowitz, M. S., Seul, M., Frisch, H. L., & McConnell, H. M. (1982) *Proc. Natl. Acad. Sci. U.S.A.* (in press).

Gaber, B. P., & Peticolas, W. K. (1977) *Biochim. Biophys. Acta 465*, 260.

Gaber, B. P., Yager, P., & Peticolas, W. L. (1978) *Biophys. J. 24*, 677.

Gebhardt, C., Gruler, H., & Sackmann, E. (1977) *Z. Naturforsch. C: Biosci. 32C*, 581.

Graddick, W. F., Stamatoff, J. B., Eisenberger, P., Berreman, D. W., & Spieldeng, N. (1979) *Biochem. Biophys. Res. Commun. 88*, 907.

Griffin, R. G. (1981) *Methods Enzymol. 72*, 108–174.

Griffin, R. G., Powers, L., & Pershan, P. S. (1978) *Biochemistry 17*, 2718.

Gupta, C. M., Radakrishnan, P., & Khorana, G. (1977) *Proc. Natl. Acad. Sci. U.S.A. 74*, 4315.

Huang, T. H., Skarjune, R. P., Wittebort, R. J., Griffin, R. G., & Oldfield, E. (1980) *J. Am. Chem. Soc. 102*, 7377.

Jacobs, R. E., & Oldfield, E. (1981) *Prog. Nucl. Magn. Reson. Spectrosc. 14*, 113.

Janiak, M. J., Small, D. M., & Shipley, G. G. (1976) *Biochemistry 15*, 4575.

Janiak, M. J., Small, D. M., & Shipley, G. G. (1979) *J. Biol. Chem. 254*, 6068.

Ladbrooke, B. D., Williams, R. M., & Chapman, D. (1968) *Biochim. Biophys. Acta 150*, 333.

Larsson, K. (1977) *Chem. Phys. Lipids 20*, 225.

Lee, A. G. (1975) *Biochim. Biophys. Acta 413*, 11.

Lee, A. G. (1977) *Biochim. Biophys. Acta 472*, 285.

Levin, I. W., & Bush, S. F. (1981) *Biochim. Biophys. Acta 640*, 760.

Linden, C. D., Wright, K. L., McConnell, H. M., & Fox, C. F. (1973) *Proc. Natl. Acad. Sci. U.S.A. 70*, 2271.

Luna, E. J., & McConnell, H. M. (1977) *Biochim. Biophys. Acta 466*, 381.

Luzzati, V. (1968) in *Biological Membranes* (Chapman, D., Ed.) Vol. 1, pp 77–121, Academic Press, London.

Mabrey, S., & Sturtevant, J. M. (1976) *Proc. Natl. Acad. Sci. U.S.A. 73*, 3862.

Mabrey, S., Mateo, P. L., & Sturtevant, J. M. (1978) *Biochemistry 17*, 2464.

Marsh, D. (1980) *Biochemistry 19*, 1632.

McIntosh, T. L. (1980) *Biophys. J. 29*, 237.

Mehring, M., Griffin, R. G., & Waugh, J. S. (1971) *J. Chem. Phys. 55*, 746.

Meier, P., Blume, A., Ohmes, E., Neugebauer, F. A., & Kothe, G. (1982) *Biochemistry 21*, 526.

Melchior, D. G., & Steim, J. M. (1979) *Prog. Surf. Membr. Sci. 13*, 211.

Mendelsohn, R., & Koch, C. C. (1980) *Biochim. Biophys. Acta 598*, 260.

Nagle, J. F. (1973) *Proc. Natl. Acad. Sci. U.S.A. 70*, 3443.

Nagle, J. F., & Wilkinson, R. A. (1978) *Biophys. J. 23*, 159.

Overath, P., & Thilo, L. (1978) *Int. Rev. Biochem. 19*, 1–44.

Overath, P., Brenner, M., Gulik-Krzywicki, T., Schechter, E., & Letellier, L. (1975) *Biochim. Biophys. Acta 389*, 358.

Owicki, J. C., & McConnell, H. M. (1980) *Biophys. J. 30*, 383.

Pearson, R. H., & Pascher, I. (1979) *Nature (London) 281*, 499.

Racker, E., Knowles, A. F., & Dytar, E. (1975) *Ann. N.Y. Acad. Sci. 264*, 17.

Rose, M. E. (1957) *Elementary Theory of Angular Momentum*, Wiley, New York.

Rubenstein, J. L. R., Smith, B. H., & McConnell, H. M. (1979) *Proc. Natl. Acad. Sci. U.S.A. 76*, 15.

Saffman, P. G., & Delbrück, M. (1975) *Proc. Natl. Acad. Sci. U.S.A. 72*, 3111.

Seelig, J. (1977) *Q. Rev. Biophys. 10*, 353.

Seelig, J., & Browning, J. L. (1978) *FEBS Lett. 92*, 41.

Seelig, J., & Seelig, A. (1980) *Q. Rev. Biophys. 13*, 19.

Sheats, J. R., & McConnell, H. M. (1978) *Proc. Natl. Acad. Sci. U.S.A. 75*, 4661.

Shimshick, E. J., & McConnell, H. M. (1973) *Biochemistry 12*, 2351.

Shinitzky, M., & Barenholz, Y. (1978) *Biochim. Biophys. Acta 515*, 367.

Shinitzky, M., Dianoux, A. C., Gitler, C., & Weber, G. (1971) *Biochemistry 10*, 2106.

Smith, B. A., & McConnell, H. M. (1978) *Proc. Natl. Acad. Sci. U.S.A. 75*, 2759.

Solomon, I. (1958) *Phys. Rev. 110*, 61.

Spiess, H. W., & Sillescu, H. (1981) *J. Magn. Reson. 42*, 381.
Stamatoff, J. B., Fever, B., Guggenheim, H., Tellez, G., & Yamane, T. (1982) *Biophys. J.* (in press).
Sunder, S., Cameron, D. G., Casal, H. L., Boulanger, Y., & Mantsch, H. H. (1981) *Chem. Phys. Lipids 28*, 137.
Tardieu, A., Luzzati, V., & Reman, F. C. (1973) *J Mol. Biol. 75*, 711.
Verkleij, A. D., Ververgaert, P. H. J., van Deenen, L. L. M., & Elbers, P. F. (1972) *Biochim. Biophys. Acta 288*, 326.
Vogel, H., & Jahnig, F. (1981) *Chem. Phys. Lipids 29*, 83.
Wittebort, R. J., Schmidt, C. F., & Griffin, R. G. (1981) *Biochemistry 20*, 4223.

Purification of a Skeletal Growth Factor from Human Bone†

John R. Farley and David J. Baylink*

ABSTRACT: A skeletal growth factor was isolated and purified from demineralized human bone matrix. A dose of 6 μg/mL of the purified factor significantly increased the proliferation rate of embryonic chick bone cells in serum-free culture (292% of controls, $p < 0.0001$) but had no effect on embryonic chick skin cells plated at the same initial density. The factor is sensitive to inactivation by trypsin and urea, but not by collagenase, 20% butanol, or 1% mercaptoethanol. It is also resistant to inactivation by heat (stable for 15 min at 75 °C) and extremes of pH (stable for 30 min at 4 °C from pH 2.5 to 10.0). Purification of the active factor by selective heat and acid precipitations, molecular sieve column chromatography, and preparative polyacrylamide gel electrophoresis provided a material that was homogeneous by the criteria of high-pressure liquid chromatography, polyacrylamide gel electrophoresis, and isoelectric focusing. The apparent molecular weight is 83 000. The purified factor increases bone cell proliferation at doses comparable to other mitogens: 0.3 μg/mL (3.6 nM) significantly increases DNA synthesis to 231% of controls ($p < 0.001$). The purified factor was also active on cultured embryonic chick bones, enhancing the growth rate of tibiae and femurs, as measured by increased dry weight (185% of controls, $p < 0.025$) and [^{3}H]proline incorporation (164% of control, $p < 0.001$), respectively.

The coupling of bone formation to resorption was first suggested by clinical observations (Harris & Heaney, 1969) and subsequently verified by in vivo studies with rats (Thompson et al., 1975; Baylink & Liu, 1979). It is our concept that this skeletal coupling provides a counterregulatory mechanism for the local control of bone volume and that faulty coupling may lead to osteoporosis (Ivey & Baylink, 1981). Previous studies from this laboratory established that (a) coupling depends on a local mechanism—it occurs in vitro (Howard et al., 1980), (b) coupling is mediated by an increase in osteoblast number (Baylink et al., 1980), (c) a factor in culture medium that has been conditioned by resorbing bone in vitro will increase both the rate of bone cell proliferation and the growth of embryonic bone (Drivdahl et al., 1980a), and (d) a similarly active factor can be extracted from embryonic chick bone (Drivdahl et al., 1980b). The factor from these latter two sources has been interpreted to be a putative coupling factor that is present in bone matrix and released by bone resorption to increase osteoblast number and thereby increase the bone formation rate. In the present studies we sought to determine whether a similar putative coupling factor was present in adult human bone matrix.

Experimental Procedures

Chemicals and Supplies. Type II collagenase was purchased from Worthington Biochemicals. BGJ_b culture medium, FCS,[1] 16-mm multiwell tissue culture plates, and all other tissue culture supplies were obtained from Gibco. Sephadex G-200 and Sephadex G-75 were purchased from Pharmacia. Acrylamide and other electrophoresis supplies, as well as ampholytes, were purchased from Bio-Rad Laboratories. [^{3}H]Proline and [^{3}H]thymidine were obtained from New England Nuclear. EGF and insulin were purchased from Collaborative Research, Inc.

Isolation and Culture of Embryonic Chick Calvarial Cells. This procedure was adapted from a method developed for the isolation of fetal rat calvarial cells (Dziak & Brand, 1974), and has been described in detail (Drivdahl et al., 1980a). Briefly, a population of cells is prepared from the frontal and parietal bones of 16-day-old embryonic chicks by sequential collagenase digestion. The cells are washed, suspended in serum-free BGJ_b medium, and plated into multiwell dishes (16-mm diameter wells) at a density of 250–350 cells/mm^2 in a total volume of 1.0 mL for incubation at 37 °C in 5% CO_2 and 95% air. For several of the experiments described below cells were plated in microwell dishes (6-mm diameter wells) at a density of 500 cells/mm^2 in a total volume of 0.25 mL. Histological examination of the calvaria before collagenase digestion showed that virtually all of the cells surrounding the embryonic bone were alkaline phosphatase positive. Since this enzyme is regarded as a specific marker for osteoblasts and their progenitors (and for chondrocytes, although they are not found in this site) (Puzas et al., 1981), we believe that the cells in these cultures are predominantly members of the osteoblast cell line. (Marrow cells and osteoclasts, which are relatively few in number, are unlikely contaminants since they are confined to the developing endosteal space which does not

† From the Department of Medicine, University of Washington, Seattle, Washington 98125, and the American Lake Veterans Administration Hospital, Tacoma, Washington 98493. *Received June 26, 1981.* This research was supported by National Institutes of Health Grants AM 27195 and DE 02600 (the latter administered by the Center for Research in Oral Biology, University of Washington) and by Veterans Administration Grant MRIS 0483.

* Address correspondence to this author at the Research Service (151), Jerry L. Pettis Memorial Veterans' Hospital, Loma Linda, CA 92357.

[1] Abbreviations: ^{3}H-TdR, tritiated thymidine; hSGF, human skeletal growth factor; cSCF, putative chick skeletal coupling factor; CM, conditioned medium; EGF, epidermal growth factor; FGF, fibroblast growth factor; FCS, fetal calf serum; BME, mercaptoethanol; IEF, isoelectric focusing; PTH, parathyroid hormone; BSA, bovine serum albumin; HSA, human serum albumin; EDTA, ethylenediaminetetraacetic acid; HPLC, high-pressure liquid chromatography.

0006-2960/82/0421-3502$01.25/0